https://doi.org/10.5194/egusphere-2024-1689
Preprint. Discussion started: 10 June 2024
© Author(s) 2024. CC BY 4.0 License.

Isolating aerosol-climate interactions in global kilometre-scale simulations

Ross J. Herbert[1,2], Andrew I. L. Williams[1,3], Philipp Weiss[1], Duncan Watson-Parris[1,4], Elisabeth Dingley[1,5], Daniel Klocke[6], and Philip Stier[1]

[1]Atmospheric Oceanic and Planetary Physics, Department of Physics, University of Oxford, Oxford, UK
[2]Now at: Institute for Climate and Atmospheric Science, University of Leeds, Leeds, UK
[3]Now at: Program in Atmospheric and Oceanic Science, Princeton University
[4]Now at: Scripps Institution of Oceanography and Halıcıoğlu Data Science Institute, University of California San Diego
[5]Now at: WCRP CMIP International Project Office
[6]Max Planck Institute for Meteorology, Hamburg, Germany

Correspondence: Ross J. Herbert (R.J.Herbert@leeds.ac.uk)

Abstract.

Anthropogenic aerosols are a primary source of uncertainty in future climate projections. Changes to aerosol concentrations modify cloud radiative properties, radiative fluxes and precipitation from the micro to the global scale. Due to computational constraints, we have been unable to explicitly simulate cloud dynamics, leaving key processes, such as convective updrafts parameterized. This has significantly limited our understanding of aerosol impacts on convective clouds and climate. However, new state-of-the-art climate models running on exascale supercomputers are capable of representing these scales. In this study, we use the kilometre-scale earth system model ICON to explore, for the first time, the global response of clouds and precipitation to anthropogenic aerosol via aerosol-cloud-interactions (ACI) and aerosol-radiation-interactions (ARI). In our month-long simulations, we find that the aerosol impact on clouds and precipitation exhibits strong regional dependence, highlighting the complex interplay with atmospheric dynamics. The impact of ARI and ACI on clouds in isolation shows some consistent behaviour, but the magnitude and additive nature of the effects are regionally dependent. This behaviour suggests that the findings of isolated case studies from regional simulations may not be representative, and that ARI and ACI processes should both be accounted for in modelling studies. The simulations also highlight some limitations to be considered in future studies. Differences in internal variability between the simulations makes large-scale comparison difficult after the initial 10 – 15 days. Longer averaging periods or ensemble simulations will be beneficial for perturbation experiments in future kilometre-scale model simulations.

1 Introduction

Aerosols and their impact on Earth's climate remain a key uncertainty for anthropogenic climate change. On the global scale, they act to primarily cool the climate, partially offsetting the warming induced by greenhouse gases (Bellouin et al., 2020; Forster et al., 2021; Watson-Parris and Smith, 2022). On the regional scale, they influence clouds, precipitation, and fluxes

https://doi.org/10.5194/egusphere-2024-1689
Preprint. Discussion started: 10 June 2024
© Author(s) 2024. CC BY 4.0 License.

of radiation throughout the atmosphere. However, the magnitude of their global and regional impact remains uncertain (Gliß et al., 2021; Myhre et al., 2018; Sand et al., 2021; Williams et al., 2022).

Aerosols modify the atmosphere via two pathways: aerosol-cloud interactions (ACI) and aerosol-radiation interactions (ARI). ACI considers the role that aerosols play in their ability to act as cloud condensation nuclei (CCN) or ice-nuclei (IN), thus directly influencing the distribution of cloud droplets or ice particles, and modifying the radiative properties of clouds and precipitation processes. ARI considers the impact that aerosols have via their radiative properties on scattering and absorption, thereby modifying the fluxes of radiation at the surface and top-of-atmosphere (TOA) and the vertical heating profile. Both ACI and ARI can interact with cloud dynamics, leading to circulation and precipitation changes.

Quantifying aerosol effects on global and regional climate is challenging due to the microphysical scales on which ACI and ARI processes fundamentally act upon, which cannot be explicitly represented in global models. A primary source of uncertainty arises in the inability for models to sufficiently represent the turbulent motions that drive the vertical transport of energy and water, which has important implications for the formation and evolution of shallow and deep-convective clouds, their diurnal cycle, and interactions between the cloud-scale and the large-scale environment. This limits our ability to accurately quantify their role in the present and future climates.

A fundamental limitation of current Earth System Models (ESMs), capable of interactively representing the atmosphere, oceans, land, and cryosphere, is their resolution, which ranges from tens to hundreds of kilometres. On these scales, fundamental climate processes, such as clouds or mesoscale ocean eddies remain unresolved and need to be parameterized. This requires the use of convection parameterizations, introducing significant uncertainties due to structural limitations such as locality (Wang et al., 2022), lack of memory (Tan et al., 2018), or the inability to accurately represent convective organisation and mesoscale convective systems (Mapes and Neale, 2011; Shamekh et al., 2023). ESMs also generally have very simplified representations of convective microphysics, as they do not explicitly represent vertical motions and associated cooling rates. A wide range of aerosol effects on convective clouds have been proposed that cannot be represented in these highly parameterized configurations. Limited area high-resolution models provide useful process insights (Marinescu et al., 2021), but their global representativeness and ability to respond to regional drivers remain unclear, and they do not satisfy large-scale controls on the availability of energy and water vapour (Dagan et al., 2022). Previous work using limited-area simulations with kilometre-scale resolution has shown that aerosols have the potential to significantly modify the diurnal cycle of convection and cloud evolution over widespread regions. This is supported by observations showing aerosol perturbations can significantly modify widespread properties of clouds through changes to the development and evolution of convection (Herbert and Stier, 2023; Jiang et al., 2018; Koren et al., 2004; Yu et al., 2007).

A new generation of global kilometre-scale models is now being developed to run on scales that explicitly simulate convection – a significant step towards a more realistic representation of the Earth system (Palmer and Stevens, 2019). The DYnamics of the Atmospheric general circulation Modeled On Non-hydrostatic Domains (DYAMOND) initiative (Stevens et al., 2019) has brought together a number of these next generation models to explore their capabilities and has demonstrated that many dynamical features in the Earth System are better reproduced with resolved convection. As such, this has greatly improved the realism (Ban et al., 2021; Kendon et al., 2019) and predictive skill (Weber and Mass, 2019) of regional precipitation magnitudes

https://doi.org/10.5194/egusphere-2024-1689
Preprint. Discussion started: 10 June 2024
© Author(s) 2024. CC BY 4.0 License.

and timings across the tropics and midlatitudes. It has also been shown to improve the representation of global scale features such as the Madden-Julian Oscillation (Savarin and Chen, 2022), demonstrating the benefits of employing these models when studying global-scale teleconnections and patterns.

Although much focus has been on convective processes and associated precipitation, the role of aerosols in these new configurations remains currently poorly understood. Many of the new generation modelling frameworks include some representation of aerosol, though their role in the climate system have only been touched upon. Sato et al. (2018), for example, studied the warm-topped cloud liquid water path (LWP) response to perturbations of the aerosol optical depth (AOD) in the NICAM model. The authors found that using an explicit representation of cloud microphysics on a global scale produced a negative LWP-AOD relationship, in agreement with satellite observations, that was not replicated in a coarser global model. The study demonstrates that ACI effects on a global-scale are sensitive to the representation of cloud processes, but did not extend the analysis to other cloud types, or consider ARI effects. It is well established that ARI can impact convective processes over land (Andreae et al., 2004; Bukowski and van den Heever, 2021; Herbert et al., 2021; Hodzic and Duvel, 2018; Jiang et al., 2018; Koren et al., 2008; Park and van den Heever, 2022) and ocean (Gordon et al., 2018; Williams et al., 2022). Therefore, it is important to understand its role alongside the improved representation of convection in these new-generation models.

The emergence of next-generation km-scale Earth System Models provides a unique opportunity to study aerosol-convection interactions and the interactions with the large-scale environment. However, at least initially, the uncertainty in explicitly simulated aerosols will remain significant, making it difficult to disentangle the complex cloud response from differences in the aerosol representation. Therefore, in this study, we examine the impact of well-defined idealized anthropogenic aerosol perturbations on the climate using global storm-resolving simulations with the ICON model (Hohenegger et al., 2023) coupled to the MACv2-SP global plume model.

2 Methodology

In this section the model and its relevant parameterization schemes are introduced. The model used for representing global distributions of natural and anthropogenic aerosols is presented, and parameterizations and methods for linking the aerosol to cloud microphysics and radiation schemes are described. Finally, we outline the simulations that we use for isolating the impact of anthropogenic aerosols on climate.

2.1 Model description and setup

The ICON model in the Sapphire configuration used here is designed for kilometre-scale simulations of the Earth system. The model is only briefly described here. A detailed description and evaluation is presented by Hohenegger et al. (2020, 2023). The atmosphere is solved with the non-hydrostatic model from Zängl et al. (2015) and land is represented with the dynamic vegetation model JSBACH (Reick et al., 2013). We run the model in atmosphere-only mode, with oceanic properties (sea surface temperature and sea ice) prescribed following the atmospheric model intercomparison project AMIP (Taylor et al., 2012). For the atmospheric flow a non-hydrostatic equation set is solved, which conserves mass, momentum and energy, as

https://doi.org/10.5194/egusphere-2024-1689
Preprint. Discussion started: 10 June 2024
© Author(s) 2024. CC BY 4.0 License.

well as parameterization schemes for the unresolved physical processes. The equations are discretized on an icosahedral-based mesh and integrated with a two-level predictor-corrector scheme.

Three parameterization schemes for radiation (Pincus et al., 2019), cloud microphysics (Baldauf et al., 2011), and turbulence (Smagorinsky, 1963) impose additional tendencies on the prognostic variables. Due to its computational complexity, the radiation scheme is called less frequently (12 min) than the cloud microphysics and turbulence schemes (40 s). Turbulence is parameterized with the Smagorinsky scheme even though turbulent eddies are only partially resolved at the kilometre-scale (Dipankar et al., 2015; Hohenegger et al., 2023; Smagorinsky, 1963). As described in the next section, idealized anthropogenic aerosols are coupled to both the radiation and cloud microphysics scheme in order to represent effects from ARI and ACI. The droplet number concentration, N_d, is used in the cloud microphysics scheme to calculate precipitation rates and in the radiation scheme to determine an effective radius. In our model configuration N_d is not coupled between the two schemes, therefore we refer to N_d separately in each scheme using the notation $N_\mathrm{d,cld}$ (cloud microphysics) and $N_\mathrm{d,rad}$ (radiation).

Radiation is parameterized with the RRTM radiative transfer scheme from Pincus et al. (2019). The scheme computes radiative properties and radiative fluxes over 14 shortwave bands from 820 to 50000 cm^{-1} and 16 longwave bands from 10 to 3250 cm^{-1}. The optical properties of clouds are sensitive to N_d, which follows a predefined vertical profile

$$N_\mathrm{d,rad} = \begin{cases} N_\mathrm{d,top} + (N_\mathrm{d,sfc} - N_\mathrm{d,top}) \exp\left(1 - (p/800\,\mathrm{hPa})^2\right), & p < 800\ \mathrm{hPa} \\ N_\mathrm{d,sfc}, \quad \text{else} \end{cases} \tag{1}$$

where $N_\mathrm{d,top}$ and $N_\mathrm{d,sfc}$ are the number concentration at the top and bottom of the atmosphere, and only used for the calculation of $N_\mathrm{d,rad}$. In our configuration, $N_\mathrm{d,top}$ is set to 20 cm^{-3} and $N_\mathrm{d,sfc}$ is dependent on the aerosol optical depth as explained in Sect. 2.2. Note that the ice crystal effective radius is dependent on ice water content alone, whereas cloud droplet effective radius (r_eff) is dependent on the cloud water content, $N_\mathrm{d,rad}$, and a scaling factor that accounts for the width of the droplet distribution (see Eq. 7 in Stevens et al. (2013)). Cloud microphysics are parameterized with the one-moment scheme from Baldauf et al. (2011). The scheme computes the masses of six water classes: water vapour, cloud water, and cloud ice as well as rain, snow, and graupel. The classes interact based on parameterized processes including condensation and autoconversion of cloud droplets to rain, the latter of which depends on N_d, i.e., $q_\mathrm{aut} \sim N_\mathrm{d,cld}^{-2}$ (Seifert and Beheng, 2006). Note that the number concentrations in the radiation and cloud microphysics schemes are not necessarily the same as they are used to tune the radiative fluxes and cloud water.

In our experiments, we use the the R02B09 grid layout, which corresponds to a horizontal grid spacing of approximately 5 km. In the vertical, the configuration has 90 levels from the surface to 75 km, with a vertical resolution ranging from ∼25 to ∼1200 m, increasing with altitude. A terrain-following hybrid coordinate formulation (SLEVE; Leuenberger et al. (2010)) is used, and a Rayleigh damping layer is applied to the top levels. The simulations are initialized using the ERA5 meteorological reanalysis and run for a 40 day period, similar to the DYAMOND protocol (Stevens et al., 2019), which includes a 10 day spin-up period. The prescribed oceanic properties are fixed at mean September values for the year 2016. The month of September is chosen due to the pronounced biomass burning activity that occurs in this month across the globe (van der Werf et al., 2017). This provides us with a large global-mean aerosol perturbation (from both absorbing and scattering aerosol), helping

https://doi.org/10.5194/egusphere-2024-1689
Preprint. Discussion started: 10 June 2024
© Author(s) 2024. CC BY 4.0 License.

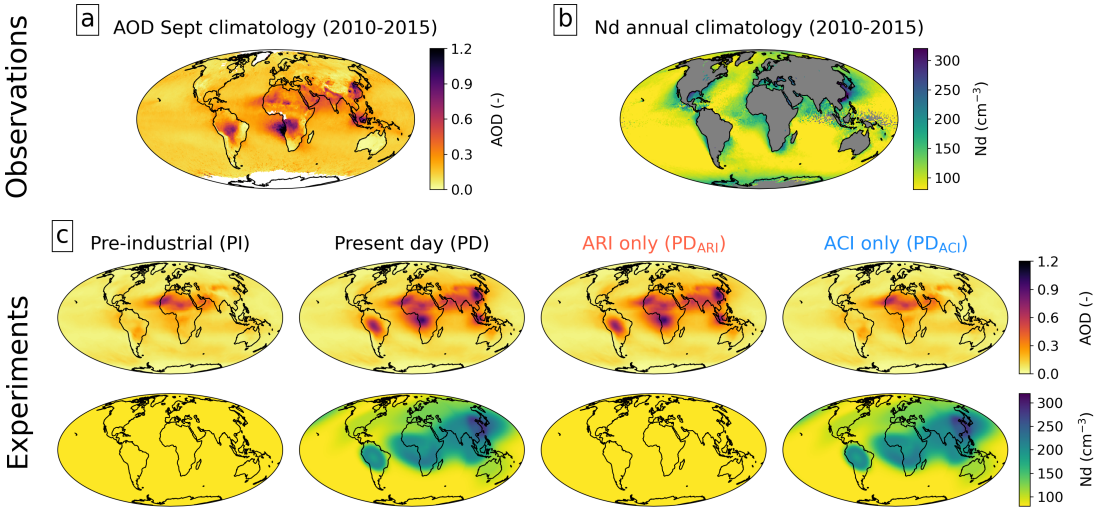

Figure 1. Climatologies of satellite retrieved (**a**) September mean $\mathrm{AOD}_{550\mathrm{nm}}$ (for 2010 - 2015) measured by Platnick et al. (2015) and (**b**) annual mean N_d over the ocean (for cloud tops < 3.2 km) estimated by Grosvenor et al. (2018). Panel (**c**) shows the idealized model AOD (top row) and $N_{\mathrm{d,cld}}$ (bottom row) in each of the 4 experiments.

to maximize the signal, and also provides valuable information on the role of absorbing aerosols in the climate system, which remain a key source of uncertainty (Bond et al., 2013; Sand et al., 2021; Williams et al., 2022). The use of fixed, monthly-mean sea surface temperatures and sea ice reduces the noise due to atmosphere-ocean coupling and permits us to focus on the rapid response of the atmosphere and climate to the aerosol perturbation, without the confounding effects of sea surface temperature changes. Aerosol perturbations, described in the following section, are held at mean September values for the year 2016 to produce a consistent aerosol perturbation throughout the simulations.

2.2 Aerosol representation

In this study, anthropogenic aerosols are represented in an idealized setting using the Max Planck Institute Aerosol Climatology version 2 Simple Plume model (MACv2-SP from Stevens et al. (2017)) with some modifications. MACv2-SP comprises a number of user-prescribed plumes, each characterized by parameters that control its horizontal and vertical distribution, aerosol concentration and optical properties, annual cycle, and long-term forcing. We use the standard setup of MACv2-SP to represent anthropogenic sources of fine-mode aerosol from nine source locations with four plumes capturing biomass burning emissions, and five capturing industrial emissions. The nine plumes are configured to reproduce the aerosol optical depth (AOD) from the Max Planck Institute Aerosol Climatology (Kinne et al., 2013) for the year 2005 and are extrapolated (as a time-dependent forcing) for use between the year 1850 to 2016.

We modify two aspects of MACv2-SP: the anthropogenic contribution to biomass burning plumes and the relationship between the AOD and cloud droplet number concentration. In the standard configuration of MACv2-SP, the biomass burning

https://doi.org/10.5194/egusphere-2024-1689
Preprint. Discussion started: 10 June 2024
© Author(s) 2024. CC BY 4.0 License.

plumes (North Africa, South America, Southeast Asia, South central Africa) have natural processes accounting for 60% of the plume AOD, and anthropogenic activities accounting for 40%. These figures are uncertain and may substantially underestimate the anthropogenic contribution (Lauk and Erb, 2009). In our simulations, we enhance the anthropogenic component to 75%, which is consistent with higher estimates and should provide a stronger signal in response to our perturbations. The spatial distribution of the droplet number concentration is calculated as

$$N_{\mathrm{d}} = a_N \ln(b_N \tau + 1), \tag{2}$$

where τ is the AOD, and a_N and b_N are predefined parameters. In the default setup as described by Stevens et al. (2017), a_N and b_N are determined using MODIS retrievals of fine-mode aerosol over the ocean regions, with values of 60 cm^{-3} and 20, respectively. This provides a very weak sensitivity of N_{d} to AOD (180 cm^{-3} for AOD of 1.0), which may be inconsistent with observations over land (Hudson and Yum, 2001; McCoy et al., 2018; Miles et al., 2000; Squires, 1958) and in the presence of convective updrafts (Braga et al., 2021; Gryspeerdt et al., 2023; Machado et al., 2018; Pringle et al., 2009) that show concentrations in excess of 300 cm^{-3}. We therefore replace the default values with those presented by Herbert et al. (2021) using in-situ observations over the Amazon rainforest to determine a relationship between N_{d} and AOD, providing values of 410 cm^{-3} and 5 for a_N and b_N. This relationship provides more sensitivity than the original used in Stevens et al. (2017), but as we show in Fig. 1 results in a present day distribution of N_{d} consistent with observations.

The global distribution of aerosols is represented using the MACv2-SP plume model, which is interfaced to the ICON radiation scheme and represents shortwave effects of ARI. Longwave effects are neglected for anthropogenic aerosols, which are predominantly sub-micron sized. In order to represent ACI in our simulations we make some minor modifications. Following the approach of Stevens et al. (2017), the relationship (2) of AOD and N_{d} is used to determine f_N as

$$f_N = \frac{N_{\mathrm{d}}}{N_{\mathrm{d,1850}}} = \frac{\ln(b_N(\tau_{1850} + \tau_{\mathrm{sp}}) + 1)}{\ln(b_N \tau_{1850} + 1)}, \tag{3}$$

where $N_{\mathrm{d,1850}}$ and N_{d} are the pre-industrial and present-day droplet number concentrations and τ_{1850} and τ_{sp} are the pre-industrial and simple-plume aerosol optical depths. In other words, the change in N_{d} from the year 1850 (representing the pre-industrial atmosphere) to present-day is determined from the change in τ over the same time period. The spatially varying factor f_N is incorporated into the cloud microphysics and radiation schemes. First, the factor modifies the number concentration used to calculate the autoconversion rate, i.e., $f_N N_{\mathrm{d,cld}}$, as outlined in Sect. 2.1. Second, the factor modifies the surface number concentration and is used to calculate the cloud optical properties, i.e., $f_N N_{\mathrm{d,sfc}}$. Note that the number concentration at the top of atmosphere ($N_{\mathrm{d,top}}$) remains unchanged. As outlined in Sect. 2.1, the radiation scheme uses $N_{\mathrm{d,rad}}$ to calculate r_{eff}.

2.3 Experiments

Simulations are designed to quantify the impact of anthropogenic aerosols on climate. The set of simulations are outlined in Table 1. A control simulation (PI) is run with a climatology of aerosols from 1850, described by Kinne (2019), representing the pre-industrial atmospheric loading of aerosol. A second simulation (PD) is performed with the MACv2-SP plume model active, producing a distribution of aerosols representative of anthropogenic aerosols in the present-day (2016) atmosphere.

https://doi.org/10.5194/egusphere-2024-1689
Preprint. Discussion started: 10 June 2024
© Author(s) 2024. CC BY 4.0 License.

Table 1. Description of each simulation.

Simulation name	ARI characteristics	ACI characteristics
PI (Pre-industrial; 1850)	AOD at pre-industrial levels	$N_{\mathrm{d,rad}}$ and $N_{\mathrm{d,cld}}$ at pre-industrial levels
PD (Present-day; ARI+ACI)	AOD increased by τ_{sp}	$N_{\mathrm{d,rad}}$ and $N_{\mathrm{d,cld}}$ increased by f_N
$\mathrm{PD_{ARI}}$ (Present-day; isolate ARI)	AOD increased by τ_{sp}	$N_{\mathrm{d,rad}}$ and $N_{\mathrm{d,cld}}$ at pre-industrial levels
$\mathrm{PD_{ACI}}$ (Present-day; isolate ACI)	AOD at pre-industrial levels	$N_{\mathrm{d,rad}}$ and $N_{\mathrm{d,cld}}$ increased by f_N

We prescribe time-independent perturbations of aerosols to remove the uncertainties associated with aerosol microphysical processes (Gliß et al., 2021; Sand et al., 2021) and instead focus on the impact of a fixed aerosol burden on the climate.

In the radiation scheme, $N_{\mathrm{d,sfc}}$ is set to 120 cm^{-3} over land and 80 cm^{-3} over oceans – the default setting in ICON. In the microphysics scheme, we use a constant $N_{\mathrm{d,cld}}$ of 80 cm^{-3} for the PI; this may not capture the distribution of naturally occurring aerosol but provides a lower limit consistent with values over remote regions (Grosvenor et al., 2018), which are likely to be more representative of the PI atmosphere. MACv2-SP is coupled independently to the radiation and cloud microphysics schemes, which provides means to isolate the role of ARI and ACI. In the ARI simulation ($\mathrm{PD_{ARI}}$), the plume model only influences the aerosol optical properties in the radiation scheme, whilst in the ACI simulation ($\mathrm{PD_{ACI}}$), the plume model influences the droplet number concentrations in the cloud microphysics and radiation schemes.

Figure 1 shows that the spatial distributions of AOD and $N_{\mathrm{d,cld}}$ across the experiments are consistent with present-day observations. In the PI, aerosols are confined to natural sources and are dominated by dust emissions over Northern Africa, biomass burning over South America and Central Africa, and sea-salt emissions over the oceans. The droplet number concentrations ($N_{\mathrm{d,cld}}$ and $N_{\mathrm{d,rad}}$) are unaffected by the scaling factor f_N. In the PD, anthropogenic aerosols are primarily centred over regions with pronounced industrial emissions of sulphate (South and East Asia, North America, and Europe) and biomass burning emissions from agricultural activities in heavily forested regions in the southern hemisphere (South America, South-Central Africa, and the Maritime Continent). $N_{\mathrm{d,cld}}$ and $N_{\mathrm{d,rad}}$ are increased by the scaling factor f_N and reach maximum concentrations of about 320 cm^{-3} over East Asia. The spatial distribution and range is consistent with present-day climatologies presented by Grosvenor et al. (2018) and McCoy et al. (2018), who report N_{d} values exceeding 300 cm^{-3} over East Asia and around 200 cm^{-3} off the coasts of the industrial regions of Asia (Fig. 1b). Elevated values are also evident over the Southeast Atlantic Ocean downwind of the African biomass burning regions. In our PD simulations, the biomass burning regions are particularly evident as we are simulating the month of September. There is a low bias over the Eastern Pacific and North Atlantic, demonstrating under-representative emissions over North America. Studies indicate aerosols in these regions have an significant effects on the sea surface temperature (Dagan et al., 2020; Fiedler and Putrasahan, 2021; Heede and Fedorov, 2021); as we are using a fixed sea surface temperature climatology we do not believe this bias will have a significant impact on the results.

https://doi.org/10.5194/egusphere-2024-1689
Preprint. Discussion started: 10 June 2024
© Author(s) 2024. CC BY 4.0 License.

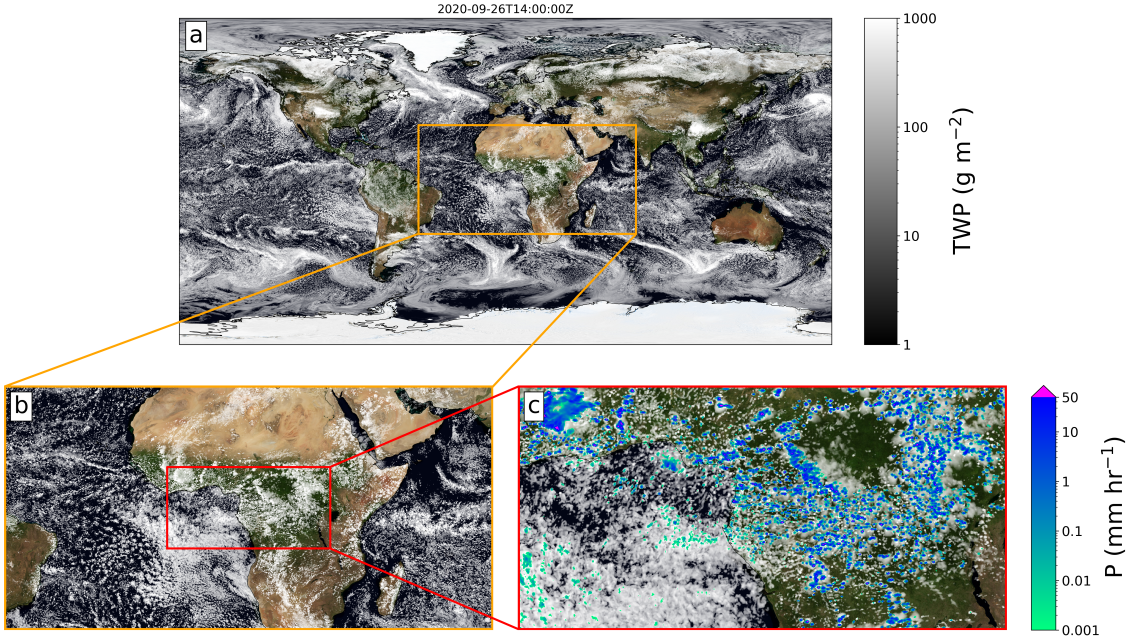

Figure 2. Snapshot of the total water path (TWP) on September 26 at 14:00 UTC for (**a**) the whole globe, (**b**) Africa and the Southeast Atlantic, and (**c**) the Congo basin in Central Africa. Panel (**c**) also includes the precipitation for rates above 0.001 mm h^{-1}. The background image in all panels is the September Blue Marble topographical composite from NASA (2024).

3 Global response

A snapshot of the model total column water path (TWP) and precipitation (P) on day 36 of the PD simulation at 14:00 UTC is shown in Fig. 2 with an increasing focus over central Africa and the Southeast Atlantic Ocean. Although the resolution is still relatively low, the figure demonstrates the ability of ICON to reproduce a variety of globally important cloud features, including the widespread regions of marine stratocumulus over the subtropical oceans, extratropical cyclones in the Northwest Pacific, the inter-tropical convergence zone (ITCZ), and long filament-like fronts in the mid-latitudes. Figure 2b shows an example of stratocumulus-to-cumulus transition as air is advected away from the coast of Africa, whilst Fig. 2c displays convection occurring over within Congo basin, with numerous deep-convective cells and the propagation of a squall-line along the edge of a large cold-pool in the centre of the image.

Snapshots from five time periods (day 2, 5, 10, 20, and 30) at 12:00 UTC during the simulations are shown in Fig. 3. The progression of the TWP response (PD - PI) demonstrates an important feature of these simulations. At the beginning of the simulation, there are widespread small-scale responses that are generally increases in TWP (clearer in the right column), especially over the Southeast Atlantic marine stratocumulus region. As the simulation progresses, the global response becomes more chaotic, especially over the mid-latitudes where non-local responses have perturbed the position and propagation of

https://doi.org/10.5194/egusphere-2024-1689
Preprint. Discussion started: 10 June 2024
© Author(s) 2024. CC BY 4.0 License.

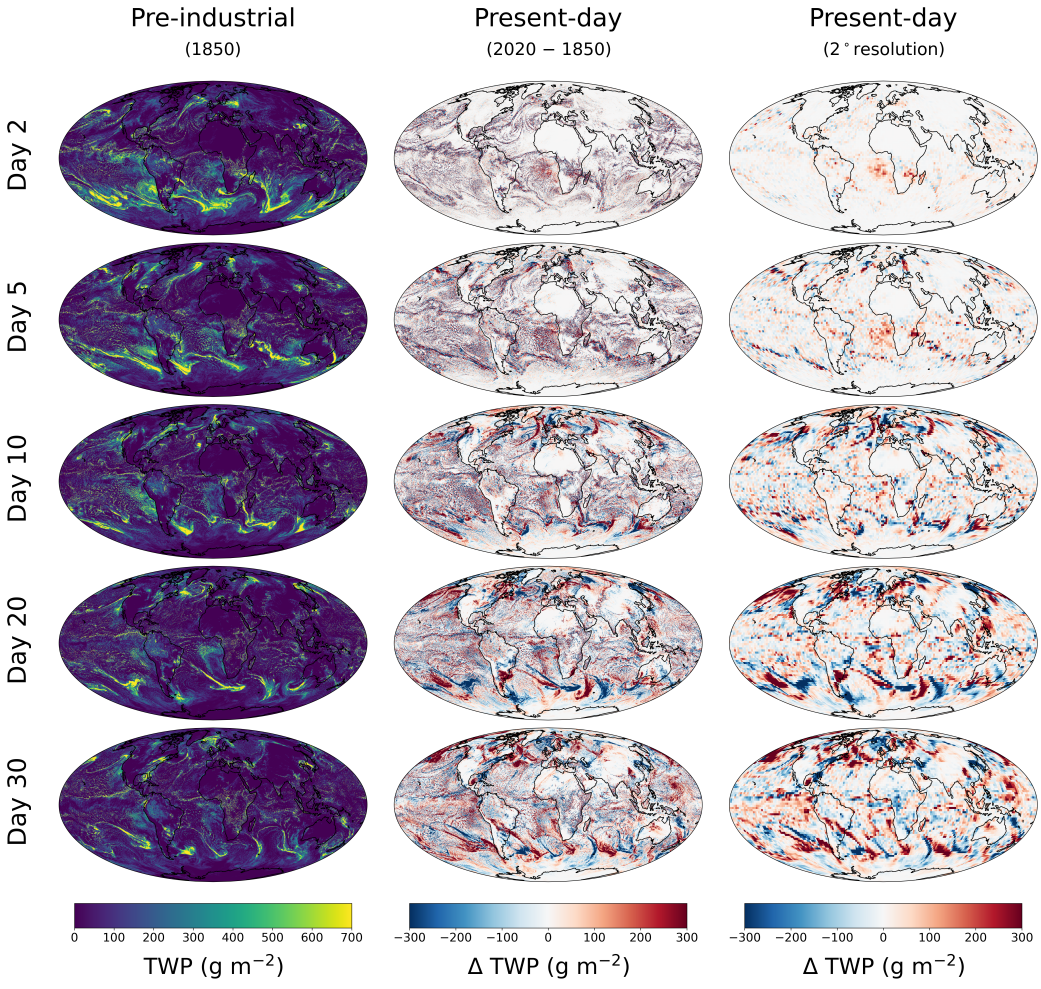

Figure 3. Snapshots of day 2, 5, 10, 20, and 30 at 12:00 UTC after the initialization: TWP in the PI simulation (left column) and response (PD - PI) to anthropogenic aerosols at native 5 km resolution (middle column) and upscaled 2-degree resolution (right column).

the Rossby waves (e.g., Sardeshmukh and Hoskins (1988)). This behaviour is similar to initial condition sensitivity where small-scale perturbations at the beginning of the simulation can quickly develop into pronounced changes (Keshtgar et al., 2023; Lorenz, 1963)). The limited length of our simulations poses some issues as it makes it difficult to disentangle this internal variability from the global-scale responses to aerosol effects. Due to this, we will only briefly discuss the global scale responses, and instead focus on the regional responses due to aerosol, allowing us to mitigate or reduce the impact of the internal variability by compositing over multiple diurnal cycles. We will revisit the issues outlined here later in the manuscript, and propose to use this study as a test-case to inform future studies.

https://doi.org/10.5194/egusphere-2024-1689
Preprint. Discussion started: 10 June 2024
© Author(s) 2024. CC BY 4.0 License.

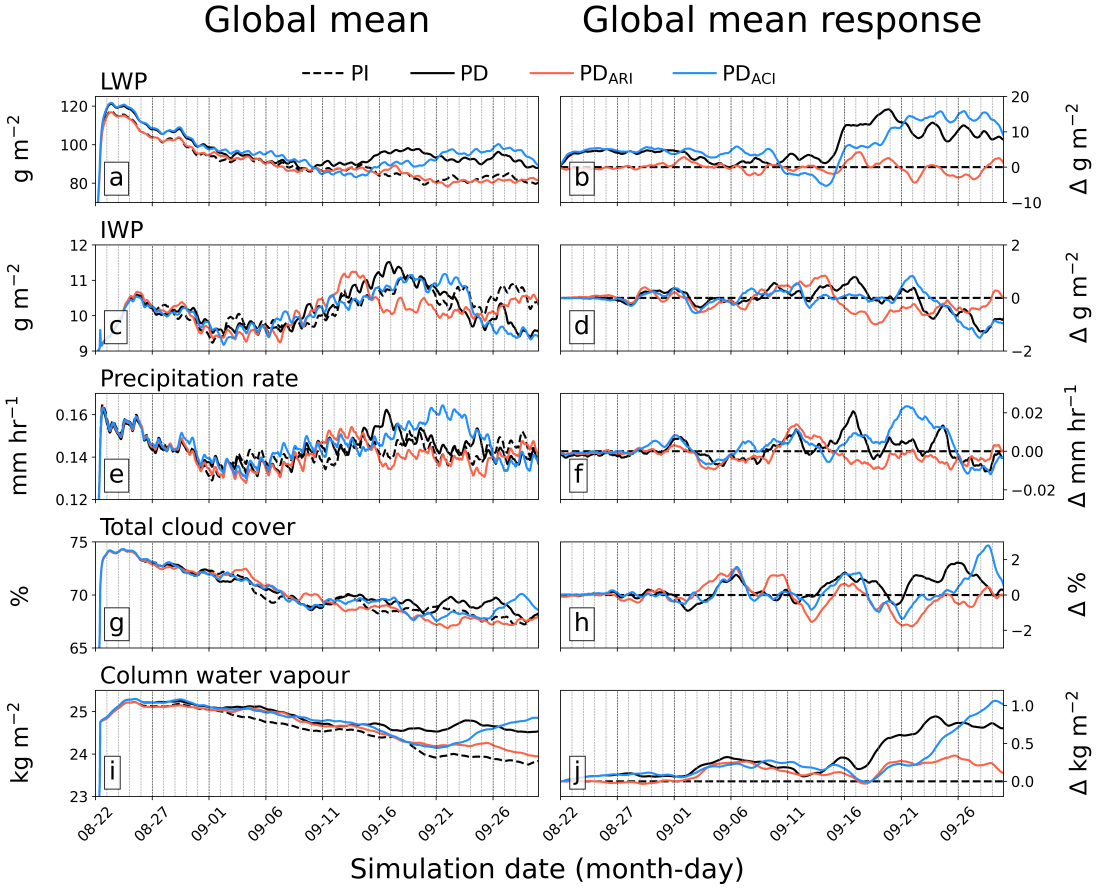

Figure 4. Time series of water species: LWP (**a** – **b**), IWP (**c** – **d**), precipitation (**e** – **f**), total cloud cover (**g** – **h**), and column integrated water vapour (**i** – **j**). Left column shows values of each simulation, and right column shows response to anthropogenic aerosols (PD_X - PI).

Figures 4 and 5 show global-mean time series of several relevant variables in each experiment alongside the mean response due to anthropogenic aerosols. The initial phase (days 1 to 5), although designed for model spin-up, provides some information on the response to aerosol. The LWP (Fig. 4b) is enhanced due to ACI by about 5 g m^{-2} with a small suppression by ARI. This is alongside a very small suppression of precipitation (Fig. 4f). This may suggest that the enhanced LWP is occurring in non- or weakly-precipitating clouds such as stratocumulus, or that there is regional variability in the precipitation response. The response of precipitation to aerosol perturbation is energetically constrained (Muller and O'Gorman, 2011; O'Gorman et al., 2012) and is known to be dependent on latitude, aerosol species, and the underlying surface (Dagan et al., 2019; Williams et al., 2023; Zhang et al., 2021). These opposing responses may be masked in the global mean, explaining the muted precipitation response in Fig. 4f. Global mean IWP and cloud cover show no response in this initial phase. As convection is strongly diurnally forced, the response may be masked due to averaging over all local times, or due to insufficient model spin-up in this

https://doi.org/10.5194/egusphere-2024-1689
Preprint. Discussion started: 10 June 2024
© Author(s) 2024. CC BY 4.0 License.

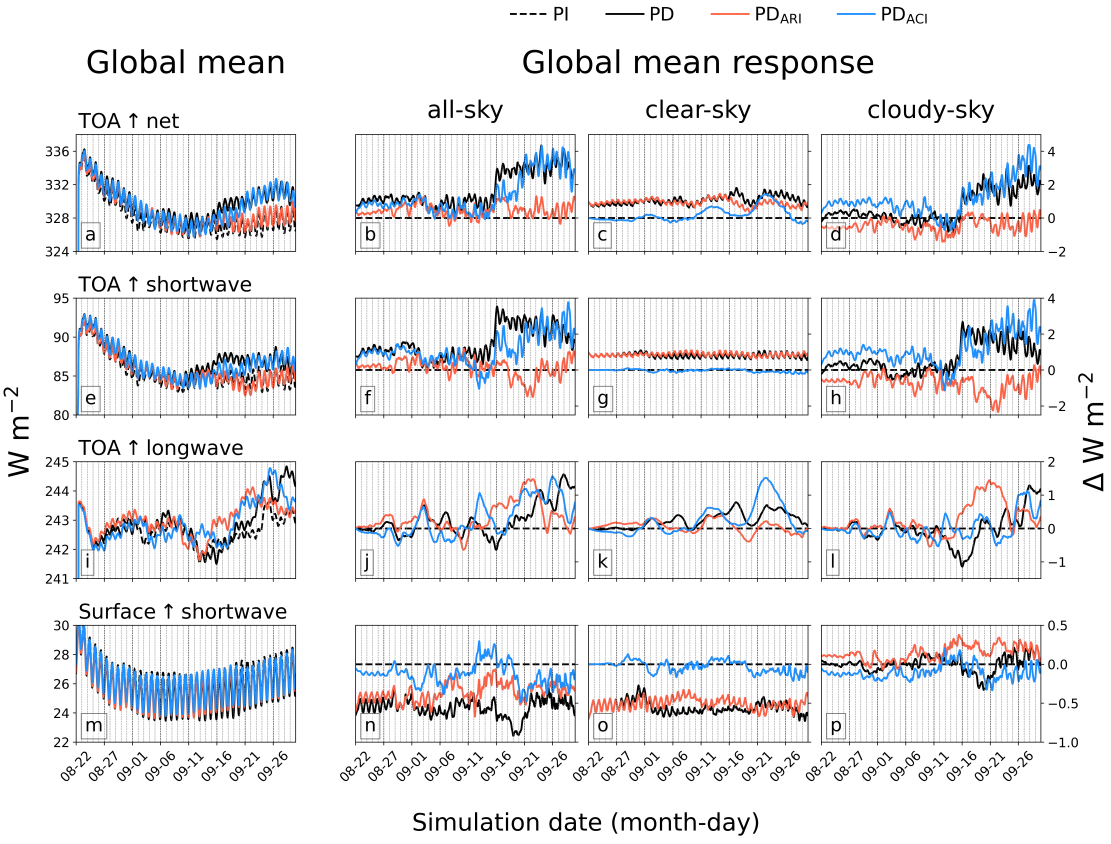

Figure 5. Time series of upward radiative fluxes: TOA net (**a** – **d**), TOA shortwave (**e** – **h**), TOA longwave (**i** – **l**), and surface shortwave (**m** – **p**). Left column shows values of each simulation, and other columns show response to anthropogenic aerosols (PD$_X$ - PI) separated into contributions from all-sky, clear-sky, and cloudy-sky fluxes (left to right).

initial phase. The LWP response, driven by ACI, persists throughout the simulation, demonstrating that even though there is considerable variability ACI remains a significant driver of enhanced LWP due to anthropogenic aerosols. This is strengthened by the similarity in time series for both PD and PD$_{ACI}$ simulations.

Figure 5 shows time series for the global mean radiative fluxes (upwards) at the top of atmosphere (TOA) and surface. Only shortwave fluxes are shown for the surface. Although the cloud property responses in Fig. 4 shows significant loss of signal due to internal variability, the radiative fluxes provide a more consistent picture. In clear-sky conditions, ARI increases outgoing shortwave radiation by about 1 W m^{-2} throughout the simulation (Fig. 5g) as a result of aerosol scattering and absorption. In clear-sky conditions, the most pronounced impact from ACI is evident in the longwave component (Fig. 5k), though this is likely due to the internal variability perturbing the global fields of water vapour. In cloudy conditions, ACI enhances cloud albedo through enhanced LWP and smaller r_{eff}, enhancing shortwave radiation throughout much of the simulation (Fig. 5h). In cloudy conditions, ARI generally reduces the net outgoing radiation by affecting the shortwave component (Fig. 5h), which

https://doi.org/10.5194/egusphere-2024-1689
Preprint. Discussion started: 10 June 2024
© Author(s) 2024. CC BY 4.0 License.

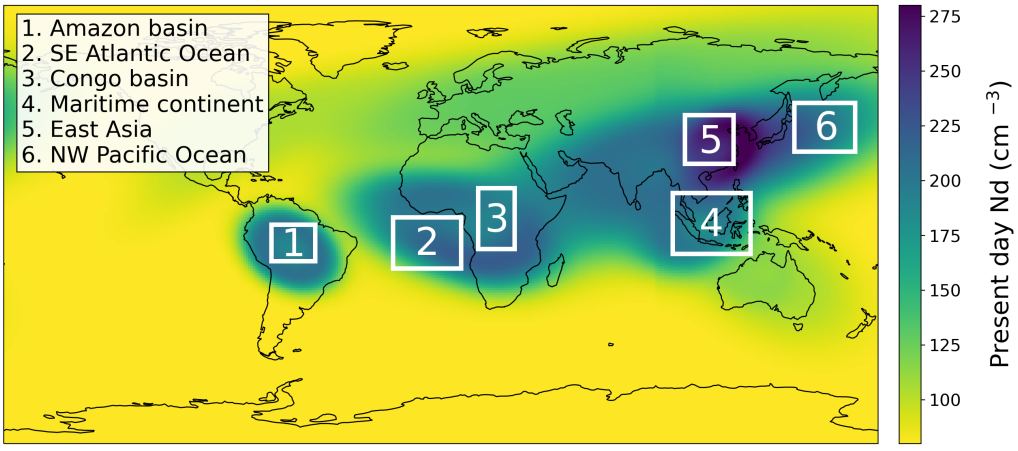

Figure 6. Domains used for the regional analysis in Sect. 4 outlined by white boxes (labeled 1 – 6). Domains are positioned over regions subject to large anthropogenic aerosol perturbations as illustrated by $N_{\mathrm{d,cld}}$ shown in the background.

may be driven by absorbing aerosol overlying clouds or suppression of clouds due to fast adjustments (semi-direct effects). The ARI cloud cover response in Fig. 4h does not show a consistent suppression, which may suggest the latter is not the primary driver or that the clouds are optically thinner. The all-sky global mean radiative response (Fig. 5b) is an increase in outgoing radiation, primarily via the shortwave component. In the initial period, the magnitude is on the order of 1 W m^{-2}, which is consistent with assessments (Bellouin et al., 2020; Forster et al., 2021), though this value increases to about 2 W m^{-2} as the simulation progresses, which is closer to upper estimates cited in those studies. Opposing signs in the TOA response for ARI in clear- and cloudy-sky conditions (Figs. 5c and d) results in ACI driving much of the observed total aerosol radiative effect. In contrast, ARI is the primary driver for changes to the surface fluxes, with a pronounced decrease in shortwave radiation driven by clear-sky conditions (Fig. 5o) as a result of aerosol extinction and reduced solar radiation reaching the surface.

The simulation configuration produces realistic cloud features, however, due to internal variability the perturbed simulations begin to diverge from the control run within ∼10 days, as expected from predictability and demonstrated by Fig. 3. As an example, we can see signs of an emerging or strengthening tropical cyclone in the Western Pacific Ocean on day 30, which will strongly dominate any signal of ACI or ARI in the region. Nonetheless, even in the global mean we find consistent responses to LWP and TOA shortwave fluxes, which we attribute to changes in cloud LWP and to direct scattering by the anthropogenic aerosol. Next we evaluate the regional and composited diurnal response of the atmosphere and bulk cloud properties to the anthropogenic aerosol. Focusing the analysis on smaller regions and compositing the time series allows us to isolate the aerosol signal, reduce the influence of internal variability that dominates the global-mean response.

https://doi.org/10.5194/egusphere-2024-1689
Preprint. Discussion started: 10 June 2024
© Author(s) 2024. CC BY 4.0 License.

Table 2. Mean AOD of each domain and change in AOD due to anthropogenic aerosols alongside the mean value of f_N.

Region (label of Fig. 6)	$\mathbf{AOD_{1850}}$	$\mathbf{\Delta AOD_{2016-1850}}$	f_N
Amazon basin (1)	0.14	0.38	3.7
SE Atlantic Ocean (2)	0.18	0.19	2.1
Congo basin (3)	0.26	0.35	2.3
Maritime Continent (4)	0.09	0.25	3.7
East Asia (5)	0.13	0.44	4.4
NW Pacific Ocean (6)	0.08	0.06	1.7

4 Regional response

In this section we focus on the regional responses to anthropogenic aerosols (regions are shown in Fig. 6). We selected the three convective regions that play a key role in shaping the tropical large-scale circulation, and three other regions heavily influenced by anthropogenic aerosols. The Amazon rainforest and the Congo basin are characteristic of continental convective regions, and are both impacted by localized biomass burning aerosol. Similarly, the Maritime Continent is impacted by biomass burning aerosol and deep convection, but situated within the globally important tropical warm pool region (De Deckker, 2016). The Southeast Atlantic Ocean and Northwest Pacific Ocean are maritime environments situated downwind of regions with strong anthropogenic aerosol emissions, and East Asia is a continental region with strong localized sulphate emissions. The novel aspect of this study is the globally resolved deep convection, hence we primarily focus on regions with deep convection.

4.1 Diurnal cycle of cloud response

Several recent studies have identified pronounced diurnal cycles in the response of clouds and their properties to aerosol perturbations, both in simulations and observations (Herbert et al., 2021; Herbert and Stier, 2023; Hodzic and Duvel, 2018). Therefore we examine the impact of PD aerosol on the regional climates by focusing on composited diurnal cycles from the whole simulation. To achieve this we decompose the regional mean time series (of each variable being examined) from day 10 onwards into short-term and long-term components. This allows us to remove the contributions by internal variability, albeit at the expense of some of the non-local impacts to the region. A seasonal-trend decomposition tool using LOESS (locally estimated scatterplot smoothing) based on Cleveland (1979) is applied to the data, providing long-term, short-term, and residual components. An example of the decomposition for the Congo basin and the Southeast Atlantic regions is shown in Fig. 7. The short-term component captures the response on a diurnal timescale, whereas the long-term component captures the internal variability combined with any persistent responses. Examples of a persistent response in a region may be a relatively warmer troposphere or enhanced subsidence. The persistent response may be an important regional impact from anthropogenic aerosol, therefore we recapture this using a second application of the decomposition tool with a large prescribed periodicity. The long-term component from the second application is retained, whilst other components from the second application are

https://doi.org/10.5194/egusphere-2024-1689
Preprint. Discussion started: 10 June 2024
© Author(s) 2024. CC BY 4.0 License.

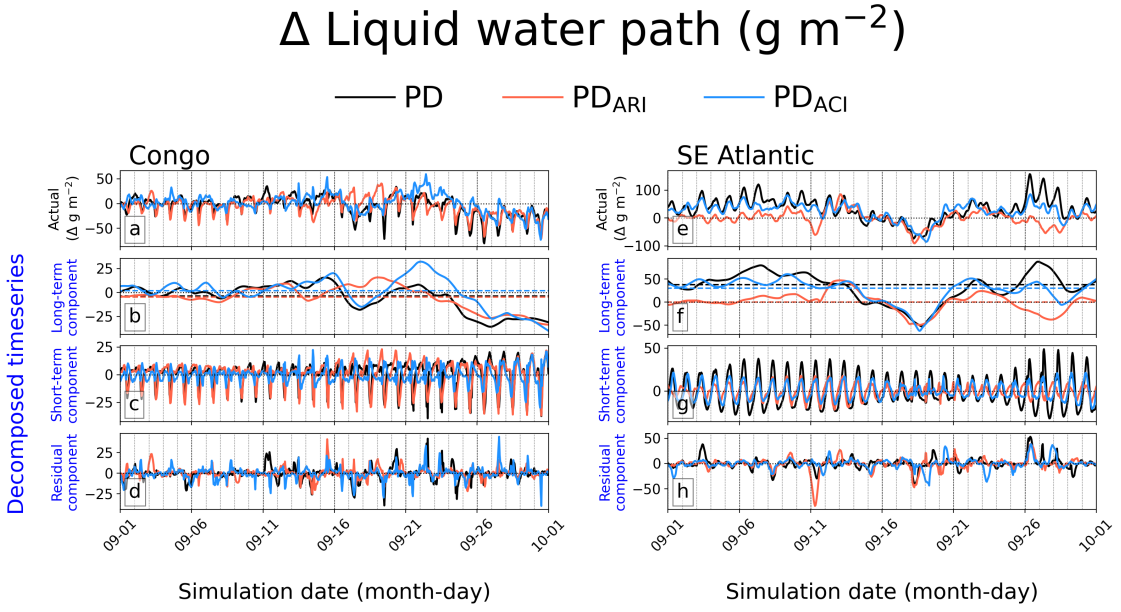

Figure 7. Example of the timescale decomposition in two regions: Congo (**a** – **d**) and Southeast Atlantic Ocean (**e** – **h**). The different colors represent the response (Δ g m^{-2}) in each PD simulation. The subplots show the original time series before decomposition (**a** and **e**), the decomposed long-term component (**b** and **f**), the decomposed short-term component (**c** and **g**), and the residual (**d** and **h**). The horizontal dashed lines (in **b** and **f**) show the underlying persistent offset that is added to the short-term component.

discarded. The recapturing of the persistent response is well-demonstrated in the Southeast Atlantic region (Figs. 7e – h). Here, ACI strongly enhances the LWP of the extensive underlying marine stratocumulus resulting in a persistent positive LWP response with an overlying diurnal cycle. To obtain an overall response from the anthropogenic aerosol perturbation we combine the short-term (diurnal) component from the first decomposition with the long-term (persistent) component from the second decomposition. The persistent response, which is independent of time, is added to the time series of the short-term component, then divided into daily time series and composited to produce a daily mean diurnal cycle of the cloud property being examined.

The composite mean diurnal cycle of LWP from each of the six regions is shown in Fig. 8. The continental convective regions (Congo, Amazon) are characterized by an afternoon peak in LWP and a somewhat smaller peak at night. The two oceanic regions (NW Pacific and SE Atlantic) have a diurnal cycle peaking overnight with the SE Atlantic region, dominated by marine stratocumulus, exhibiting a pronounced minimum during the day. The Maritime Continent displays characteristics of both the continental convective regions and the oceanic regions, with LWP peaks in the morning and afternoon. East Asia has a less well-defined LWP diurnal cycle though some of this might be lost in the considerable internal variability evident in the decomposed time series (Fig. 8e). All regions demonstrate strong sensitivity to PD aerosol perturbations, though each displays unique characteristics. We start with responses to ARI and ACI in isolation, and then discuss the combined effects.

https://doi.org/10.5194/egusphere-2024-1689
Preprint. Discussion started: 10 June 2024
© Author(s) 2024. CC BY 4.0 License.

The primary response of the atmosphere in each region due to the isolated ARI pathway (PD_{ARI}) is a modification to the large-scale dynamical properties. In the convective regions (Congo, Amazon, Maritime Continent) ARI consistently suppresses LWP between 12:00 and 15:00 LST (e.g., Fig. 8a), which coincides with the initiation and evolution of deep convective cells, thus indicating that ARI from absorbing aerosol suppresses deep convection. This is consistent with modelling studies over the Amazon (Herbert et al., 2021; Liu et al., 2020; Martins et al., 2009) and Indonesia (Hodzic and Duvel, 2018). The widespread impact of biomass burning aerosol on the diurnal cycle of resolved convection via ARI has not been previously studied over central Africa. We provide evidence that this region is similarly sensitive with pronounced suppression of convection due to ARI. These simulations suggest that in regions dominated by biomass burning aerosol, ARI consistently impacts deep convection via suppressed activity during the afternoon. However, the magnitude of the LWP suppression is region-dependent, ranging between -12% (Maritime Continent), -29% (Congo), and -33% (Amazon). This sensitivity may be due to the background conditions of the convective environment (Williams et al., 2022), the different aerosol plume characteristics, or buffering of the response due to coupling to large-scale meteorology. The Maritime Continent includes both land and ocean, so the relatively weaker sensitivity may be a result of a difference in the relative suppression of convection between land and (at least partly) ocean. The SE Atlantic displays a small LWP suppression during the daytime and enhancement overnight, with an overall negligible daily-mean effect. Marine stratocumulus clouds in this region are known to be sensitive to the vertical structure of temperature, moisture, and biomass burning aerosol (Herbert et al., 2020; Koch and Del Genio, 2010; Wood, 2012), which exhibits more complexity than is represented by our idealized plume and model vertical resolution. Additionally, a lack of feedback to sea surface fluxes may be suppressing the cloud response to ARI. East Asia demonstrates a diurnal cycle in the response similar to the convective regions, and the NW Pacific shows a persistent enhancement of LWP. However, these two regions are heavily influenced by natural variability as observed by the day-to-day variability of the daily diurnal cycle (Figs. 8d and e), limiting our ability to isolate the underlying impacts.

In this model configuration, ACI directly influences the production of precipitation (via autoconversion) and thereby LWP. The response of LWP to anthropogenic aerosol via the ACI pathway (PD_{ACI}) generally follows this pathway, with overall enhancements observed in most regions. The continental convective regions have an increased LWP during the day, coinciding with the initiation of deep convection. This is consistent with Herbert et al. (2021) who showed that deeper clouds, with greater condensate loading, are more sensitive to ACI. Over the Maritime Continent there is an additional enhancement of LWP throughout the diurnal cycle of +10%. This reflects the prevalence of low-level marine clouds over much of this region (Fig. 6) and may be partially driven by enhanced cloud cover (Sect. 3). The Congo and the Amazon do not have this persistent enhancement, reflecting the dominance of deep convection for driving the diurnal cycle of LWP. The SE Atlantic, characterized by widespread low-level stratocumulus, displays a strong and robust LWP enhancement due to ACI reaching +25% at night with very little day-to-day variability. East Asia and the NW Pacific both similarly show persistent enhancements of LWP though there is considerable day-to-day variability, again, reflecting the natural variability observed in these regions.

When ARI and ACI pathways are isolated in the PD_{ARI} and PD_{ACI} experiments the cloud LWP responses are consistent across all regions. However, when both ARI and ACI pathways are active in the PD experiment the overall LWP response is unique to each region. This suggests a degree of regionally-dependent non-linearity between ARI and ACI. The overall LWP

https://doi.org/10.5194/egusphere-2024-1689
Preprint. Discussion started: 10 June 2024
© Author(s) 2024. CC BY 4.0 License.

response over the Congo is driven by ARI with very little role from ACI, whereas over the Amazon the overall response is largely a linear combination of the isolated ARI and ACI responses. In the Amazon region, the timing of the isolated ACI response suggests that ARI is driving reductions in deep convection, but ACI is impacting the resulting properties of the clouds that form - thereby explaining the overall response of LWP. Herbert et al. (2021) found that isolated ACI and ARI cloud responses were active in separate cloud regimes over the convective environment of the Amazon rainforest, with ACI evident in shallow cumulus, and ARI more evident in deep convective processes. This difference may stem from the microphysics scheme used in the study, and will be discussed further in Sect. 5. In the Maritime Continent the overall LWP response is a linear sum of ARI and ACI responses during the afternoon, but is non-linear overnight into the morning. The SE Atlantic region also displays non-linearity in the response, with enhanced LWP greater than the sum of the two isolated pathways most pronounced during the morning. The similarities of the two regions suggests the non-linearity is occurring in the shallow marine clouds and may be associated with a positive feedback. The NW Pacific and East Asia regions show non-linearity in the opposite direction, with the overall LWP response being weaker than the sum of the two isolated pathways. However, given the natural variability here it is not possible to say whether this is an appropriate conclusion.

4.2 Response of convection and cloud vertical profiles

In Figures 9 – 11 we focus on the drivers of the cloud response to anthropogenic aerosol in the three convective regions. Given their similarities we will analyse the Amazon and Congo first, followed by the Maritime Continent. Deep convective clouds play an important role in the hydrological cycle, and can strongly perturb fluxes of radiation at the surface and TOA. Figure 9 shows the mean diurnal response of ice water path (IWP), cloud mass flux (M_{flux}), and precipitation for the three regions. The mass flux is taken at 500 hPa and constrained to regions with ascending airmasses. Figure 10 shows regional mean vertical profiles of liquid (LWC) and ice (IWC) with responses decomposed into the local morning (AM) and afternoon (PM) time periods to isolate any diurnal variability. Figure 11 shows mean profiles of large-scale thermodynamic properties in the region: vertical velocity in grid cells with ascending air ($w_{\uparrow}$), potential temperature (θ), and specific humidity (q_v). The profiles shown in Figs. 10 and 11 have not been decomposed so will include influences from internal variability.

4.2.1 Continental convective regions

The Amazon and Congo regions display strong similarities in the LWP response due to the isolated ACI and ARI effects but differ in the linearity of the combined effects (Figs. 8a – b). We start by focusing on each pathway (PD_{ARI} and PD_{ACI}) followed by the overall effect (PD).

The timing of the LWP response due to ARI ($\sim$ 14:00 LST) in the PD_{ARI} experiment suggests suppression of deep convection. This is supported by a 30% and 20% reduction in M_{flux} for the Congo and Amazon regions between 12:00 and 15:00 LST with weakened $w_{\uparrow}$ throughout much of the column in the afternoon (PM) period. The profiles of θ and q_v in Fig. 11 for PD_{ARI} in isolation show that the strongly absorbing aerosol produces localized heating of the smoke layer, suppressing BL mixing and drying aloft. Suppressed convection reduces the vertical extent of clouds, resulting in decreased LWC throughout the column (Fig. 10). A similar change in AOD over the Congo and Amazon (Table 2) results in a comparable suppression in M_{flux} ($\sim$

https://doi.org/10.5194/egusphere-2024-1689
Preprint. Discussion started: 10 June 2024
© Author(s) 2024. CC BY 4.0 License.

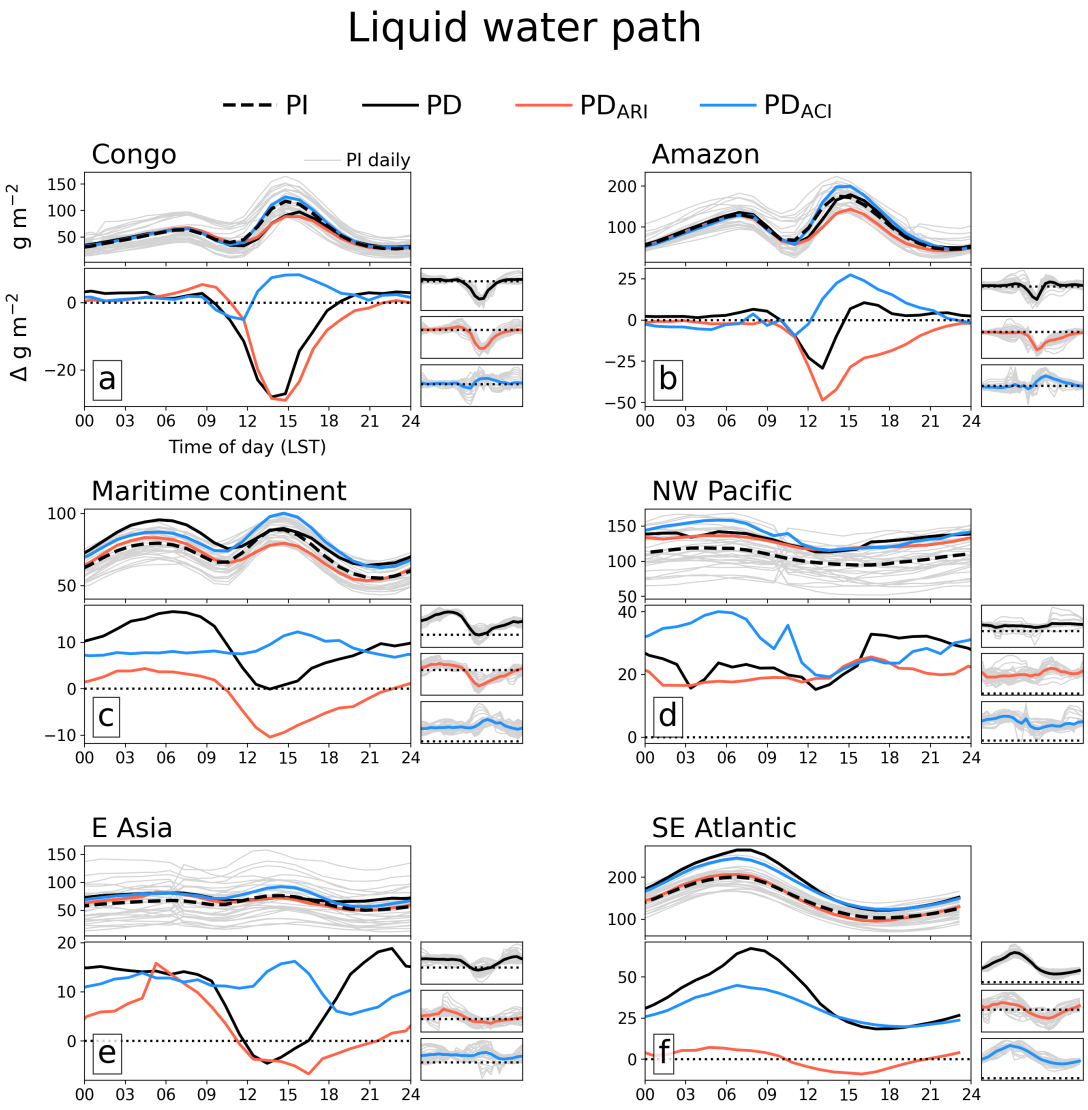

Figure 8. Composites of decomposed diurnal response of LWP over the six regions of interest. For each region (**a** – **f**) the top sub-plot shows the mean diurnal cycle of LWP (g m^{-2}) in each simulation, with grey lines showing each day of the PI simulation. The lower sub-plots show the PD response (Δ g m^{-2}) to aerosol perturbations in each simulation (PD$_X$ - PI), which are repeated individually to the right along with grey lines showing each day of the composite.

360 30 and 20%). This is consistent with the findings of Herbert et al. (2021). However, the response of the $w_\uparrow$ profile and LWP is more pronounced over the Amazon and suggests the differences may be due to stronger capacity to buffer the perturbation over the Congo, which tends to exhibit more convection than the Amazon in all experiments. Changes to convection and the vertical transport of condensate also impacts cold-phase cloud properties. Both regions display a strong suppression of IWP

https://doi.org/10.5194/egusphere-2024-1689
Preprint. Discussion started: 10 June 2024
© Author(s) 2024. CC BY 4.0 License.

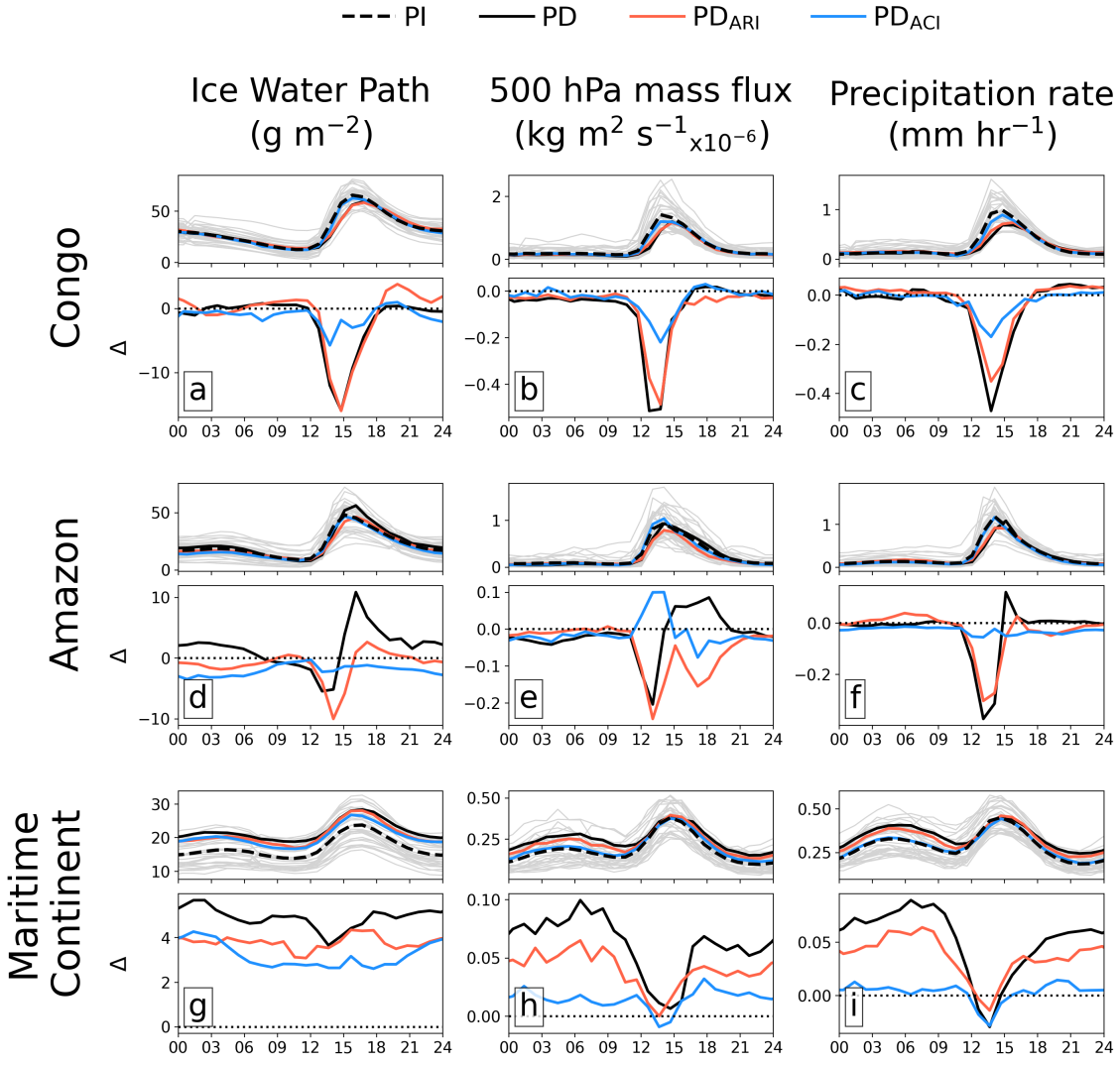

Figure 9. Composites of diurnal response in the three convective regions for ice water path (**a**, **d**, and **g**), cloud condensate mass flux at 500 hPa (**b**, **e**, and **h**), and precipitation rate (**c**, **f**, and **i**). See Fig. 8 for a description of each subplot.

during the afternoon (Fig. 9), with a smaller enhancement during the evening. The IWC vertical profiles (Fig. 10) show a small increase at the top of the cloudy columns, and more extensive decreases below. This may be explained by weaker convective cells that reduce the transport of condensate to the freezing level. The increase in IWP during the evening and the increase in high altitude ice may be explained by a delayed release of convective available potential energy (CAPE). Given that mean M_{flux} over the regions does not increase overnight, this may suggest the occurrence of fewer, but more intense, convective cells that occur slightly later in the afternoon. Wu et al. (2011) reported an increase in CAPE aloft due to ARI in simulations over the Amazon, supporting this theory.

https://doi.org/10.5194/egusphere-2024-1689
Preprint. Discussion started: 10 June 2024
© Author(s) 2024. CC BY 4.0 License.

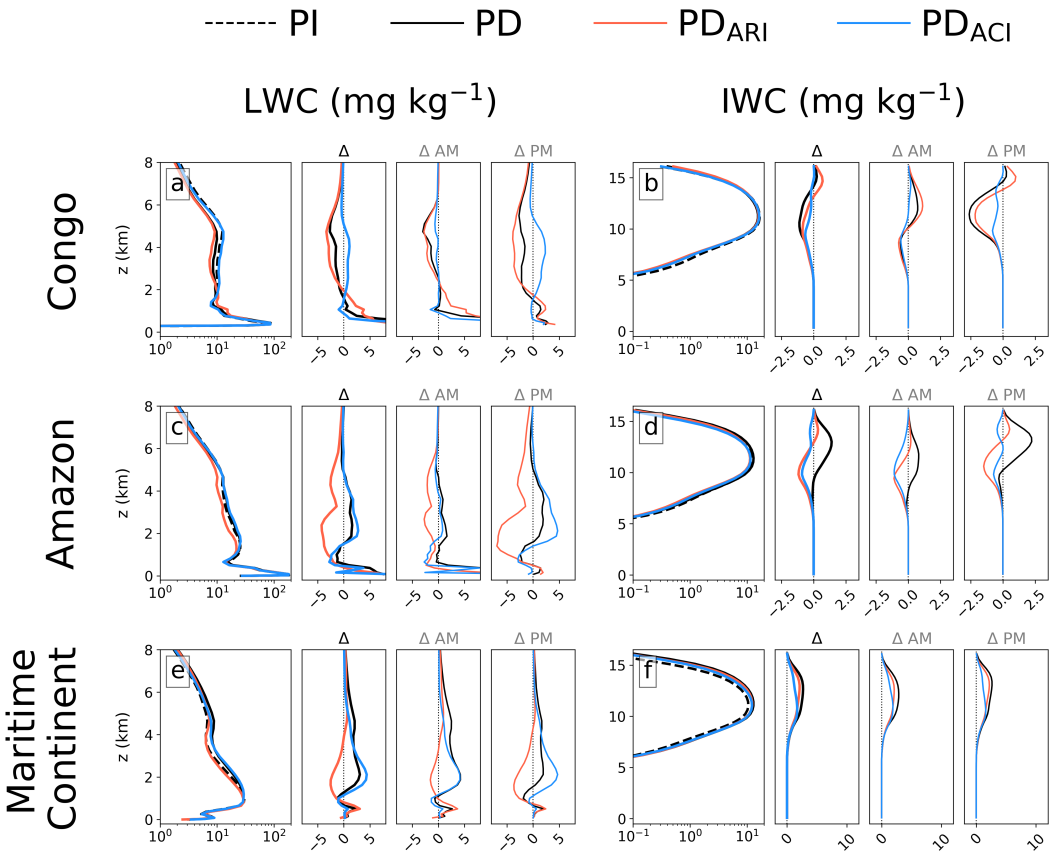

Figure 10. Mean vertical profiles of LWC (**a**, **c**, and **e**) and IWC (**b**, **d**, and **f**). Each plot (**a** – **f**) shows from left to right: absolute mean profile for the last 30 days of the simulation; diurnal mean response (PD$_X$ - PI); mean response during the AM (00:00 to 12:00 LST); and mean response during the PM (12:00 - 24:00 LST). Note that the LWC is shown from 0 to 8 km altitude, whereas IWC is shown from 0 to 16 km altitude.

Figure 10 demonstrates that the ACI pathway drives a redistribution of liquid water towards the top of the deep clouds. An increase in LWP and a decrease in precipitation for PD$_{ACI}$ in the afternoon (Fig. 9) is consistent with suppression of the warm rain process that could be enhanced by additional release of latent heat from condensation (‘*warm invigoration*’ e.g., Lebo (2014); Sheffield et al. (2015); Fan et al. (2018)). In both regions there are also signs of enhanced low-level cloud LWC (below 1 km), and suppressed IWC throughout the column. There is an overall decrease in vertical ascent in both regions, though it is difficult to separate the contributions from the deep convective cells and large-scale ascending regions. A weak suppression of convection via ACI was reported by Herbert et al. (2021), primarily occurring within weaker updraft cores, and also in the model intercomparison of Marinescu et al. (2021) - though only for some of the models.

The two continental regions respond in a similar manner to the individual pathways of ARI and ACI, but there are differences in the overall effect (contrasting PD experiment with PD$_{ACI}$ and PD$_{ARI}$). In the Congo region ACI drives the overall response of

https://doi.org/10.5194/egusphere-2024-1689
Preprint. Discussion started: 10 June 2024
© Author(s) 2024. CC BY 4.0 License.

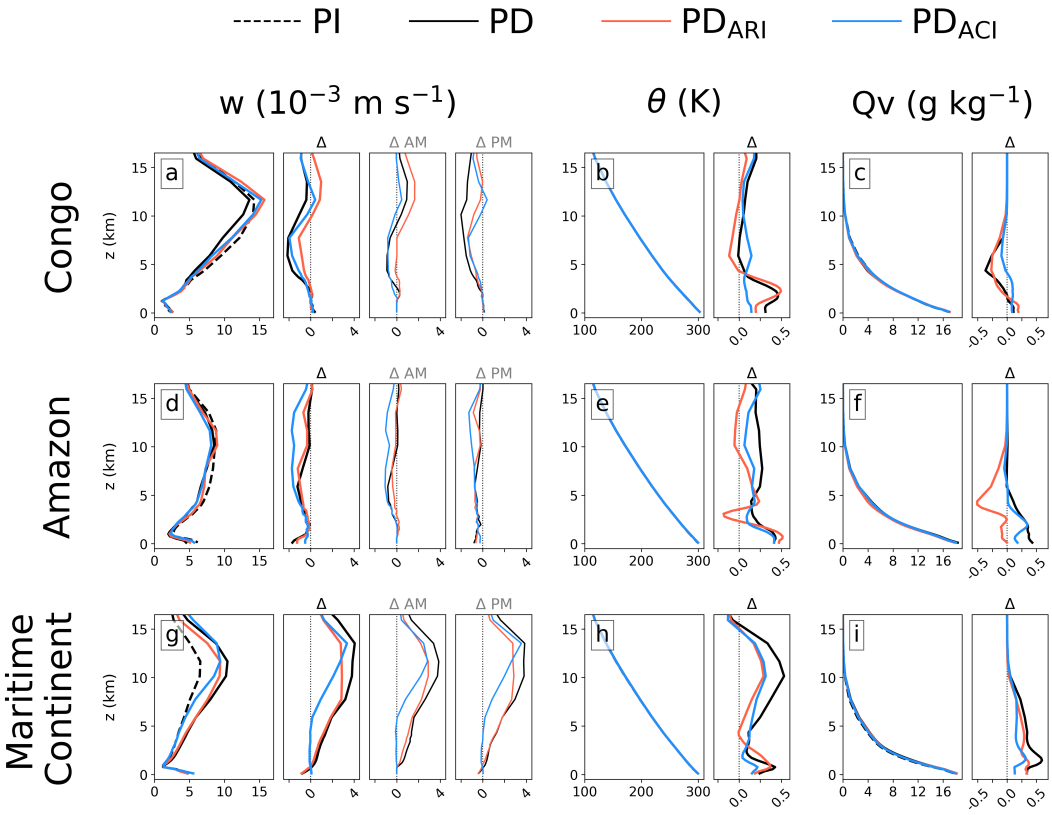

Figure 11. Same analysis as in Fig. 10, but for vertical mean profiles of ascending vertical velocity (**a**, **d**, and **g**), potential temperature (**b**, **e**, and **h**), and specific humidity (**c**, **f** and **i**). Morning (AM) and afternoon (PM) mean responses are only shown for vertical velocity.

the low (< 2 km) clouds, whilst ARI drives the overall response of the deeper clouds (Fig. 10). The thermodynamic properties of the region (Fig. 11) show a largely combined effect from the two pathways for all variables, which suggests the properties of the low-altitude clouds play an important role in modifying the environment away from deep convective clouds. Though both pathways play a role in the vertical profile of cloud response, it is ARI that ultimately drives most of the regional cloud response (LWP, IWP, and precipitation) due to the dominating presence of deeper convective clouds in the Congo region (Figs. 10a and 11a).

In the Amazon region the decomposed diurnal cycles and profiles show a less consistent picture. The most robust feature is the overall suppression in LWP, IWP, M_{flux}, and precipitation between 12:00 and 15:00 LST (and some recovery overnight) primarily driven by ARI and to a lesser extent ACI. In the afternoon and early evening period the overall response is often stronger than the sum of the two pathways (most notably M_{flux}, IWP, and precipitation). This may be explained by a non-linear response where delayed CAPE (via ARI) combines with enhanced condensate loading (via ACI) to enhance the amount of water reaching the freezing level and high-altitude cloud coverage. The LWP response also shows evidence that the overall

https://doi.org/10.5194/egusphere-2024-1689
Preprint. Discussion started: 10 June 2024
© Author(s) 2024. CC BY 4.0 License.

response is strongly influenced by both ARI and ACI. However, in contrast to the Congo region, ACI plays a stronger role in the Amazon. This could be explained by the Amazonian cloud field containing relatively more shallow convection than in the Congo (Fig. 10), which is a regime known to be sensitive to ACI (Langton et al., 2021). This suggests the response of convective regions to changes in the aerosol population is dependent on the background state, which has also been observed in remote-sensing studies of the Amazon region (Herbert and Stier, 2023; Ten Hoeve et al., 2011; Yu et al., 2007).

This analysis suggests the Congo and Amazon are strongly perturbed by anthropogenic aerosol from biomass burning sources. The primary driver is a localized modification to the convective environment that reduces daily accumulated precipitation by 1 mm day^{-1} in both regions ($\sim$ 15% and 10% of PI values for Congo and Amazon). This is consistent with Barkhordarian et al. (2019) who report a long-term drying of the Amazon partially driven by changes to cloudiness and precipitation patterns they associate with biomass burning aerosol. Long-term trends are not observed over the Congo region, but decadal-scale rainfall trends in Western Africa have been shown to be sensitive to aerosol in GCMs (Zhang et al., 2021), manifesting as a slow response mediated by large-scale adjustments of the atmosphere and sea surface temperature. This study suggests the modification to deep convection may have an additional impact on precipitation over the region which is unlikely to be represented in GCMs. Additionally, non-local sources of moisture have been found to be important for driving convective activity in these regions (Creese and Washington, 2018; Wu and Lee, 2019), which suggests both scales (convection permitting resolution and large-scale drivers) need to be represented in order to fully capture the impact of anthropogenic aerosol and greenhouse gases on precipitation trends over continental convective regions. We propose that extended (month- to annual-scale) global storm-resolving simulations should become a key tool for such process based investigations.

4.2.2 The Maritime Continent

The response of the cloud field over the Maritime Continent shows consistent behaviour with the other convective regions, but in contrast, the anthropogenic aerosol impacts the large-scale circulation. This is evident from substantial persistent responses in the cloud properties throughout the diurnal cycle that are combined with the time-dependent responses observed in Sect. 4.2.1. The decomposed diurnal cycles in Fig. 9 show evidence that, relative to persistent responses, the ARI pathway suppresses M_{flux} between 12:00 and 15:00 LST alongside a local minimum in LWP (Fig. 8c) and precipitation. LWC at 500 hPa shows little change (Fig. 10e), suggesting the suppressed M_{flux} is related to weakened convection. The ACI pathway also suppresses M_{flux} at this time period, whilst enhancing LWP. These isolated impacts from ARI and ACI to the initiation and scale of deep convection are consistent with the other two regions.

Over the Maritime Continent the ARI pathway is associated with an persistent increase in M_{flux} by $\sim$ 20 %, primarily driven by enhanced ascent (Fig. 11g) that extends throughout the column. The anomalous and persistent ascent drives enhanced LWC in the lower troposphere (shallow cumulus) but produces drying aloft and enhanced IWC (Fig. 10). This suggests that the ARI pathway is simultaneously impacting both large-scale circulation and local-scale convection. The response of the large-scale circulation to ARI is consistent with the strengthening of the Walker Circulation and tropical ascent reported by Williams et al. (2022), where the anomalous source of diabatic heating projects onto the ascending branch of the Walker Circulation. Williams et al. (2022) did not investigate the diurnal cycle, but used a model with parameterized convection to demonstrate

https://doi.org/10.5194/egusphere-2024-1689
Preprint. Discussion started: 10 June 2024
© Author(s) 2024. CC BY 4.0 License.

that absorbing aerosol over this region drives increased ascent in the mean state. Here we build on this by using a model with explicit deep convection, which additionally reveals an important role for the diurnal cycle of convection and precipitation.

The response of mass flux and precipitation to the ACI pathway in isolation is weaker than ARI over the Maritime Continent, but there is a relatively stronger impact on LWP and therefore the radiative effect. M_{flux} and precipitation responds weakly (Fig. 9) whereas there is a pronounced and constant increase (throughout diurnal cycle) of LWP (by $\sim 20\,\%$) and IWP ($\sim 25\,\%$). These responses occur alongside an increase in vertical velocity (Fig. 11g) above ~ 6 km, which may occur in the convective cells and/or the large-scale ascending circulation. The profiles in Fig. 10 show enhanced IWC aloft with little coincident LWC response, and Fig. 11h shows that there is an associated region of enhanced θ comparable to that from ARI. This may point towards invigoration of the ascending cloudy air (Marinescu et al., 2021).

The overall response of the region to anthropogenic aerosol is driven by both ARI and ACI, with some properties of the cloud and atmosphere being dominated by one of the pathways. The diurnal cycles of LWP, M_{flux}, and precipitation are approximately a linear sum of the contributions from the two pathways. During the AM period the LWC profile response is controlled by ACI effects, whilst during the PM time period both ARI and ACI contribute to the changes - illustrating the connection between ARI and deep convection over the land. ARI dominates the response of w in the warm-phase regions of the cloud, and ACI in the ice-phase regions (Fig. 11g). This highlights that the Maritime Continent may be particularly sensitive to anthropogenic aerosol due to its position within the Walker circulation and the pronounced diurnal cycle of convection. It is possible that other regions within ascending or descending branches of global atmospheric circulation may exhibit similar sensitivity (Williams et al., 2022) and should be considered in future studies.

5 Conclusions

In this study we make the first steps towards investigating the impact of anthropogenic aerosol on clouds, precipitation and radiation in a global kilometre-scale configuration of the ICON model. Month-long simulations at convection permitting resolution with idealized aerosol plumes allow us to demonstrate the potential of global kilometre-scale models for studying aerosol impacts on clouds across spatial scales from the microphysical, through the synoptic, and into the global scale. As a community, we know that aerosol perturbations drive complex responses and feedbacks across scales (Stier et al., 2024), but previously it has been necessary to focus on limited regional domains to capture the features that drive the formation and evolution of clouds, and their response to aerosols.

We focus on the cloud and climate response to a prescribed aerosol perturbation, which we represent using the MACv2-SP plume model. This allows us to link aerosol perturbations to changes in radiative fluxes and cloud droplet number concentration. We ran simulations for the month of September, both for PI and PD aerosol distributions, providing a realistic range of perturbations across the globe. Additional PD simulations were run to isolate the response of the clouds to ARI and ACI pathways.

The global mean response of bulk cloud properties in the initial 10 days (designed as the spin-up period) shows an enhancement of LWP and column water vapour due to ACI, with little impact from ARI, and signs of marginally suppressed

https://doi.org/10.5194/egusphere-2024-1689
Preprint. Discussion started: 10 June 2024
© Author(s) 2024. CC BY 4.0 License.

precipitation. IWP and cloud cover shows little response to either pathway. Following this initial period, the global mean response in cloud properties exhibit no persistent response except for LWP and column water vapour which remain enhanced via ACI. Inspection of global maps highlights the role of internal variability, with synoptic-scale weather systems diverging around 10 days into the simulation. This is expected from predictability, as random small-scale differences between the pairs of simulations will propagate with time (Lorenz, 1963; Keshtgar et al., 2023), developing into pronounced differences. Upscaling the analysis to a coarser resolution of 2 degree highlights the recovery of some features (Fig. 3) and a possible future direction. The high resolution is necessary for accurately representing simulated cloud behaviour, whereas for the analysis of these simulations it is the regional to global-scale response that is of primary importance.

Amidst the internal variability there are consistent responses that emerge through the radiative fluxes in cloudy- and clear-sky conditions. Surface and TOA fluxes are strongly impacted by ARI in the clear-sky, but largely balanced by opposing responses in cloudy regions with cloud thickening (ACI) and rapid adjustments (ARI). The net effect is an increase in outgoing radiation between 1 and 2 $\mathrm{W\,m^{-2}}$. The higher value is within upper estimates of the radiative effect of anthropogenic aerosol (Bellouin et al., 2020; Forster et al., 2021) and is maintained throughout the last 15 days of the simulation. If this is driven by changes in cloud-scale properties (resolved by the convection permitting resolution) rather than internal variability, then this would represent an important result to explore in future studies. Clearly, reducing the degree of internal variability is required. This could be achieved via longer simulations (e.g., Bolot et al. (2023); Cheng et al. (2022); Sato et al. (2018) or ensembles (e.g., Deser et al. (2020); Dittus et al. (2020). However, this will require considerable computing resources. Sato et al. (2018) ran a year-long global kilometre-scale simulation using the NICAM model and analysed ACI by focusing on the global relationship between LWP and the aerosol number concentration, removing the need to run multiple simulations. An alternative is to nudge the simulation to observed meteorology (e.g., Atlas et al. (2022, 2024); Terai et al. (2020). However, this will suppress any large-scale modifications to the atmospheric thermodynamics and circulation, which as observed in this study, may be an important feature in some regions.

Previous studies have demonstrated the impact of aerosol perturbations on the diurnal cycle of cloud properties. Hence, the global mean response may be masking important diurnal features. We investigated this by focusing on six regions impacted by anthropogenic aerosol and decomposed the month-long time series to produce composite diurnal cycles of cloud responses. Three regions characterized by deep convection amidst absorbing aerosol demonstrated suppressed convection due to ARI and enhanced LWP due to ACI, though the combined effect differed in each region. Similarly, the IWP and precipitation responses were not consistent. We hypothesize that the differences are a result of the large-scale thermodynamic environment and surface properties (continental vs maritime) unique to each region, manifesting as a state dependence in the response to the aerosol. Additionally, large-scale responses were evident in the Indo-Pacific warm pool region in the ascending branch of the Walker circulation, driving changes to the large-scale circulation alongside the cloud-scale response. The results point towards strong regional dependence in the impact of aerosols on clouds and climate, hence the outcomes from isolated case studies are likely not representative for other regions. The results also strongly suggest that ACI and ARI cannot be considered independently as the responses via each pathway does not tend to be additive. Some were dominated by either ACI or ARI, and some behaved non-linearly, resulting in a response at odds with the individual components.

https://doi.org/10.5194/egusphere-2024-1689
Preprint. Discussion started: 10 June 2024
© Author(s) 2024. CC BY 4.0 License.

In these simulations we use prescribed fields of aerosol. This gives us the opportunity to focus on aerosol impacts without the added uncertainties associated with aerosol microphysics, transport and removal, yet may be masking important feedbacks and processes. This includes the strong impact of clouds and precipitation on the spatio-temporal distribution of aerosols, changes to the surface properties, fluxes and turbulence that would influence emissions and aerosol removal processes. An additional source of uncertainty is from the cloud microphysics scheme. In a model intercomparison study on aerosol effects on deep convection, Marinescu et al. (2021) report significant variability of the simulated convective base state as well as the ACI response between models, in particular of the impact on updraught characteristics. The choice of the cloud microphysics can also greatly impact the response of convective clouds to aerosol (Heikenfeld et al., 2019; White et al., 2017), as can the representation of cold-phase processes (Sullivan and Voigt, 2021). A key reason for the model and microphysics uncertainty is the lack of observational constraints for cloud microphysical processes, in particular in convective updrafts (Johnson et al., 2015; Pathak et al., 2020; Proske et al., 2023).

Constraints will be required for evaluating and developing future global kilometre-scale simulations of aerosol-climate interactions. Intensive field campaigns targeting aerosol-convection interactions such as the Tracking Aerosol Convection interactions ExpeRiment (TRACER) and associated campaigns (e.g., Lappin et al. (2023)), will provide valuable observations, and will complement previous field campaigns (e.g., GoAmazon (Martin et al., 2016), ACRIDICON-CHUVA (Wendisch et al., 2016), and CACTI (Varble et al., 2021)). However, there is a lack of intensive field-campaign observations from the convective regions of Africa and Southeast Asia. These regions exhibit sensitivity to anthropogenic aerosol and would benefit from additional observations. Existing remote-observation platforms (e.g., AQUA, TERRA, and CloudSat) will soon be joined by ESA's Earth Cloud Aerosol and Radiation Explorer (EarthCARE; Illingworth et al. (2015)) and NASA's Plankton Aerosol Clouds and Ecosystems (PACE; Gorman et al. (2019)) satellite. These new missions, focusing on aerosols and clouds, will be a useful addition and help continue the long-term observational record of aerosols in the earth system. This is especially timely given the recent cessation of CloudSat.

This study revealed significant aerosol effects on convective clouds and climate and a complex interplay of local effects with the regional and global circulation. However, these effects remain subject to significant model uncertainties. To understand and reduce these uncertainties, the GEWEX Aerosol Precipitation (GAP) initiative (https://www.gewex.org/GAP/) is organising a global kilometre-scale model intercomparison study, building on the idealized aerosol perturbation setup established in this work.

While this work improves our understanding of climate and circulation responses to idealized aerosol perturbations, its simplicity limits the representativeness for realistic aerosol perturbations. This gap will be closed by future aerosol perturbation experiments in global kilometre-scale models with an interactive treatment of aerosols and clouds. The required tools are currently being developed in initiatives such as nextGEMS funded through the European Union (Weiss et al., 2023; Weiss and Stier, 2024) or EAGLES funded through the Department of Energy (Ma, 2024). It would be beneficial to extend such simulations to multi-decadal time-scales; this would reduce the signal of inter-annual variability, and reduce the uncertainty associated with quantifying the role of anthropogenic aerosols on clouds, precipitation, and climate.

https://doi.org/10.5194/egusphere-2024-1689
Preprint. Discussion started: 10 June 2024
© Author(s) 2024. CC BY 4.0 License.

Code and data availability. All data relevant for producing figures and necessary python scripts are available on Zenodo at https://zenodo.org/records/11470778 (Herbert, 2024).

Author contributions. PS conceptualized the research. RJH, AILW, PW, DWP and PS designed the methodology and experiments. RJH, AILW, PW and DK prepared and ran the simulations. RJH and PW processed and analysed the simulation output. RJH prepared the manuscript with contributions from all co-authors.

Competing interests. At least one of the (co-)authors is a member of the editorial board of Atmospheric Chemistry and Physics.

Acknowledgements. This research was supported by the European Research Council project RECAP under the European Union's Horizon 2020 research and innovation programme (grant no. 724602) and by the FORCeS project under the European Union's Horizon 2020 research programme with grant agreement no. 821205. PS additionally acknowledges funding from the European Union's Horizon 2020 project nextGEMS under grant agreement number 101003470 and the European Union's Horizon Europe project CleanCloud with grant agreement 101137639 and its UKRI underwrite. AILW acknowledges funding from the CIMES Postdoctoral Fellowship under award NA18OAR4320123 from the National Oceanic and Atmospheric Administration, U.S. Department of Commerce. We thank the German Climate Computing Center (DKRZ) for use of its computer facilities on which the simulations were performed.

https://doi.org/10.5194/egusphere-2024-1689
Preprint. Discussion started: 10 June 2024
© Author(s) 2024. CC BY 4.0 License.

References

Andreae, M. O., Rosenfeld, D., Artaxo, P., Costa, A. A., Frank, G. P., Longo, K. M., and Silva-Dias, M. A.: Smoking Rain Clouds over the Amazon, Science, 303, 1337–1342, https://doi.org/10.1126/science.1092779, publisher: American Association for the Advancement of Science, 2004.

Atlas, R. L., Bretherton, C. S., Khairoutdinov, M. F., and Blossey, P. N.: Hallett-Mossop Rime Splintering Dims Cumulus Clouds Over the Southern Ocean: New Insight From Nudged Global Storm-Resolving Simulations, AGU Advances, 3, e2021AV000454, https://doi.org/10.1029/2021AV000454, _eprint: https://onlinelibrary.wiley.com/doi/pdf/10.1029/2021AV000454, 2022.

Atlas, R. L., Bretherton, C. S., Sokol, A. B., Blossey, P. N., and Khairoutdinov, M. F.: Tropical Cirrus Are Highly Sensitive to Ice Microphysics Within a Nudged Global Storm-Resolving Model, Geophysical Research Letters, 51, e2023GL105868, https://doi.org/10.1029/2023GL105868, _eprint: https://onlinelibrary.wiley.com/doi/pdf/10.1029/2023GL105868, 2024.

Baldauf, M., Seifert, A., Förstner, J., Majewski, D., Raschendorfer, M., and Reinhardt, T.: Operational Convective-Scale Numerical Weather Prediction with the COSMO Model: Description and Sensitivities, Monthly Weather Review, 139, 3887–3905, https://doi.org/10.1175/MWR-D-10-05013.1, publisher: American Meteorological Society Section: Monthly Weather Review, 2011.

Ban, N., Caillaud, C., Coppola, E., Pichelli, E., Sobolowski, S., Adinolfi, M., Ahrens, B., Alias, A., Anders, I., Bastin, S., Belušić, D., Berthou, S., Brisson, E., Cardoso, R. M., Chan, S. C., Christensen, O. B., Fernández, J., Fita, L., Frisius, T., Gašparac, G., Giorgi, F., Goergen, K., Haugen, J. E., Hodnebrog, Ø., Kartsios, S., Katragkou, E., Kendon, E. J., Keuler, K., Lavin-Gullon, A., Lenderink, G., Leutwyler, D., Lorenz, T., Maraun, D., Mercogliano, P., Milovac, J., Panitz, H.-J., Raffa, M., Remedio, A. R., Schär, C., Soares, P. M. M., Srnec, L., Steensen, B. M., Stocchi, P., Tölle, M. H., Truhetz, H., Vergara-Temprado, J., de Vries, H., Warrach-Sagi, K., Wulfmeyer, V., and Zander, M. J.: The first multi-model ensemble of regional climate simulations at kilometer-scale resolution, part I: evaluation of precipitation, Climate Dynamics, 57, 275–302, https://doi.org/10.1007/s00382-021-05708-w, 2021.

Barkhordarian, A., Saatchi, S. S., Behrangi, A., Loikith, P. C., and Mechoso, C. R.: A Recent Systematic Increase in Vapor Pressure Deficit over Tropical South America, Scientific Reports, 9, 15331, https://doi.org/10.1038/s41598-019-51857-8, number: 1 Publisher: Nature Publishing Group, 2019.

Bellouin, N., Quaas, J., Gryspeerdt, E., Kinne, S., Stier, P., Watson-Parris, D., Boucher, O., Carslaw, K. S., Christensen, M., Daniau, A.-L., Dufresne, J.-L., Feingold, G., Fiedler, S., Forster, P., Gettelman, A., Haywood, J. M., Lohmann, U., Malavelle, F., Mauritsen, T., McCoy, D. T., Myhre, G., Mülmenstädt, J., Neubauer, D., Possner, A., Rugenstein, M., Sato, Y., Schulz, M., Schwartz, S. E., Sourdeval, O., Storelvmo, T., Toll, V., Winker, D., and Stevens, B.: Bounding Global Aerosol Radiative Forcing of Climate Change, Reviews of Geophysics, 58, e2019RG000660, https://doi.org/10.1029/2019RG000660, _eprint: https://onlinelibrary.wiley.com/doi/pdf/10.1029/2019RG000660, 2020.

Bolot, M., Harris, L. M., Cheng, K.-Y., Merlis, T. M., Blossey, P. N., Bretherton, C. S., Clark, S. K., Kaltenbaugh, A., Zhou, L., and Fueglistaler, S.: Kilometer-scale global warming simulations and active sensors reveal changes in tropical deep convection, npj Climate and Atmospheric Science, 6, 1–8, https://doi.org/10.1038/s41612-023-00525-w, number: 1 Publisher: Nature Publishing Group, 2023.

Bond, T. C., Doherty, S. J., Fahey, D. W., Forster, P. M., Berntsen, T., DeAngelo, B. J., Flanner, M. G., Ghan, S., Kärcher, B., Koch, D., Kinne, S., Kondo, Y., Quinn, P. K., Sarofim, M. C., Schultz, M. G., Schulz, M., Venkataraman, C., Zhang, H., Zhang, S., Bellouin, N., Guttikunda, S. K., Hopke, P. K., Jacobson, M. Z., Kaiser, J. W., Klimont, Z., Lohmann, U., Schwarz, J. P., Shindell, D., Storelvmo, T., Warren, S. G., and Zender, C. S.: Bounding the role of black carbon in the climate system: A scientific assessment, Journal of Geophysical Research: Atmospheres, 118, 5380–5552, https://doi.org/10.1002/jgrd.50171, 2013.

https://doi.org/10.5194/egusphere-2024-1689
Preprint. Discussion started: 10 June 2024
© Author(s) 2024. CC BY 4.0 License.

Braga, R. C., Ervens, B., Rosenfeld, D., Andreae, M. O., Förster, J.-D., Fütterer, D., Hernández Pardo, L., Holanda, B. A., Jurkat-Witschas, T., Krüger, O. O., Lauer, O., Machado, L. A. T., Pöhlker, C., Sauer, D., Voigt, C., Walser, A., Wendisch, M., Pöschl, U., and Pöhlker, M. L.: Cloud droplet formation at the base of tropical convective clouds: closure between modeling and measurement results of ACRIDICON–CHUVA, Atmospheric Chemistry and Physics, 21, 17 513–17 528, https://doi.org/10.5194/acp-21-17513-2021, publisher: Copernicus GmbH, 2021.

Bukowski, J. and van den Heever, S. C.: Direct Radiative Effects in Haboobs, Journal of Geophysical Research: Atmospheres, 126, e2021JD034 814, https://doi.org/10.1029/2021JD034814, _eprint: https://onlinelibrary.wiley.com/doi/pdf/10.1029/2021JD034814, 2021.

Cheng, K.-Y., Harris, L., Bretherton, C., Merlis, T. M., Bolot, M., Zhou, L., Kaltenbaugh, A., Clark, S., and Fueglistaler, S.: Impact of Warmer Sea Surface Temperature on the Global Pattern of Intense Convection: Insights From a Global Storm Resolving Model, Geophysical Research Letters, 49, e2022GL099 796, https://doi.org/10.1029/2022GL099796, _eprint: https://onlinelibrary.wiley.com/doi/pdf/10.1029/2022GL099796, 2022.

Cleveland, W. S.: Robust Locally Weighted Regression and Smoothing Scatterplots, Journal of the American Statistical Association, 74, 829–836, https://doi.org/10.1080/01621459.1979.10481038, publisher: Taylor & Francis _eprint: https://www.tandfonline.com/doi/pdf/10.1080/01621459.1979.10481038, 1979.

Creese, A. and Washington, R.: A Process-Based Assessment of CMIP5 Rainfall in the Congo Basin: The September–November Rainy Season, Journal of Climate, 31, 7417–7439, https://doi.org/10.1175/JCLI-D-17-0818.1, publisher: American Meteorological Society Section: Journal of Climate, 2018.

Dagan, G., Stier, P., and Watson-Parris, D.: Analysis of the Atmospheric Water Budget for Elucidating the Spatial Scale of Precipitation Changes Under Climate Change, Geophysical Research Letters, 46, 10 504–10 511, https://doi.org/10.1029/2019GL084173, publisher: Blackwell Publishing Ltd, 2019.

Dagan, G., Stier, P., and Watson-Parris, D.: Aerosol Forcing Masks and Delays the Formation of the North Atlantic Warming Hole by Three Decades, Geophysical Research Letters, 47, e2020GL090 778, https://doi.org/10.1029/2020GL090778, _eprint: https://onlinelibrary.wiley.com/doi/pdf/10.1029/2020GL090778, 2020.

Dagan, G., Stier, P., Spill, G., Herbert, R., Heikenfeld, M., Van Den Heever, S. C., and Marinescu, P. J.: Boundary conditions representation can determine simulated aerosol effects on convective cloud fields, Communications Earth & Environment, 3, 71, https://doi.org/10.1038/s43247-022-00399-5, 2022.

De Deckker, P.: The Indo-Pacific Warm Pool: critical to world oceanography and world climate, Geoscience Letters, 3, 20, https://doi.org/10.1186/s40562-016-0054-3, 2016.

Deser, C., Phillips, A. S., Simpson, I. R., Rosenbloom, N., Coleman, D., Lehner, F., Pendergrass, A. G., DiNezio, P., and Stevenson, S.: Isolating the Evolving Contributions of Anthropogenic Aerosols and Greenhouse Gases: A New CESM1 Large Ensemble Community Resource, Journal of Climate, 33, 7835–7858, https://doi.org/10.1175/JCLI-D-20-0123.1, 2020.

Dipankar, A., Stevens, B., Heinze, R., Moseley, C., Zängl, G., Giorgetta, M., and Brdar, S.: Large eddy simulation using the general circulation model ICON, Journal of Advances in Modeling Earth Systems, 7, 963–986, https://doi.org/10.1002/2015MS000431, _eprint: https://onlinelibrary.wiley.com/doi/pdf/10.1002/2015MS000431, 2015.

Dittus, A. J., Hawkins, E., Wilcox, L. J., Sutton, R. T., Smith, C. J., Andrews, M. B., and Forster, P. M.: Sensitivity of Historical Climate Simulations to Uncertain Aerosol Forcing, Geophysical Research Letters, 47, e2019GL085 806, https://doi.org/10.1029/2019GL085806, _eprint: https://onlinelibrary.wiley.com/doi/pdf/10.1029/2019GL085806, 2020.

https://doi.org/10.5194/egusphere-2024-1689
Preprint. Discussion started: 10 June 2024
© Author(s) 2024. CC BY 4.0 License.

Fan, J., Rosenfeld, D., Zhang, Y., Giangrande, S. E., Li, Z., Machado, L. A., Martin, S. T., Yang, Y., Wang, J., Artaxo, P., Barbosa, H. M., Braga, R. C., Comstock, J. M., Feng, Z., Gao, W., Gomes, H. B., Mei, F., Pöhlker, C., Pöhlker, M. L., Pöschl, U., and De Souza, R. A.: Substantial convection and precipitation enhancements by ultrafine aerosol particles, Science, 359, 411–418, https://doi.org/10.1126/science.aan8461, publisher: American Association for the Advancement of Science, 2018.

Fiedler, S. and Putrasahan, D.: How Does the North Atlantic SST Pattern Respond to Anthropogenic Aerosols in the 1970s and 2000s?, Geophysical Research Letters, 48, e2020GL092 142, https://doi.org/10.1029/2020GL092142, _eprint: https://onlinelibrary.wiley.com/doi/pdf/10.1029/2020GL092142, 2021.

Forster, P., Storelvmo, T., Armour, K., Collins, W., Dufresne, J.-L., Frame, D., Lunt, J, D., Mauritsen, T., Palmer, D, M., Watanabe, M., Wild, M., and Zhang, H.: The Earth's Energy Budget, Climate Feedbacks, and Climate Sensitivity, in: Climate Change 2021: The Physical Science Basis. Contribution of Working Group I to the Sixth Assessment Report of the Intergovernmental Panel on Climate Change, pp. 923–1054, Cambridge University Press, Cambridge, United Kingdom and New York, NY, USA, doi:10.1017/9781009157896.009, 2021.

Gliß, J., Mortier, A., Schulz, M., Andrews, E., Balkanski, Y., Bauer, S. E., Benedictow, A. M. K., Bian, H., Checa-Garcia, R., Chin, M., Ginoux, P., Griesfeller, J. J., Heckel, A., Kipling, Z., Kirkevåg, A., Kokkola, H., Laj, P., Le Sager, P., Lund, M. T., Lund Myhre, C., Matsui, H., Myhre, G., Neubauer, D., van Noije, T., North, P., Olivié, D. J. L., Rémy, S., Sogacheva, L., Takemura, T., Tsigaridis, K., and Tsyro, S. G.: AeroCom phase III multi-model evaluation of the aerosol life cycle and optical properties using ground- and space-based remote sensing as well as surface in situ observations, Atmospheric Chemistry and Physics, 21, 87–128, https://doi.org/10.5194/acp-21-87-2021, publisher: Copernicus GmbH, 2021.

Gordon, H., Field, P. R., Abel, S. J., Dalvi, M., Grosvenor, D. P., Hill, A. A., Johnson, B. T., Miltenberger, A. K., Yoshioka, M., and Carslaw, K. S.: Large simulated radiative effects of smoke in the south-east Atlantic, Atmospheric Chemistry and Physics, 18, 15 261–15 289, https://doi.org/10.5194/acp-18-15261-2018, 2018.

Gorman, E. T., Kubalak, D. A., Patel, D., Dress, A., Mott, D. B., Meister, G., and Werdell, P. J.: The NASA Plankton, Aerosol, Cloud, ocean Ecosystem (PACE) mission: an emerging era of global, hyperspectral Earth system remote sensing, in: Sensors, Systems, and Next-Generation Satellites XXIII, edited by Neeck, S. P., Martimort, P., and Kimura, T., vol. 11151, p. 111510G, International Society for Optics and Photonics, SPIE, https://doi.org/10.1117/12.2537146, 2019.

Grosvenor, D. P., Sourdeval, O., Zuidema, P., Ackerman, A., Alexandrov, M. D., Bennartz, R., Boers, R., Cairns, B., Chiu, J. C., Christensen, M., Deneke, H., Diamond, M., Feingold, G., Fridlind, A., Hünerbein, A., Knist, C., Kollias, P., Marshak, A., McCoy, D., Merk, D., Painemal, D., Rausch, J., Rosenfeld, D., Russchenberg, H., Seifert, P., Sinclair, K., Stier, P., van Diedenhoven, B., Wendisch, M., Werner, F., Wood, R., Zhang, Z., and Quaas, J.: Remote Sensing of Droplet Number Concentration in Warm Clouds: A Review of the Current State of Knowledge and Perspectives, Reviews of Geophysics, 56, 409–453, https://doi.org/10.1029/2017RG000593, _eprint: https://onlinelibrary.wiley.com/doi/pdf/10.1029/2017RG000593, 2018.

Gryspeerdt, E., Povey, A. C., Grainger, R. G., Hasekamp, O., Hsu, N. C., Mulcahy, J. P., Sayer, A. M., and Sorooshian, A.: Uncertainty in aerosol–cloud radiative forcing is driven by clean conditions, Atmospheric Chemistry and Physics, 23, 4115–4122, https://doi.org/10.5194/acp-23-4115-2023, publisher: Copernicus GmbH, 2023.

Heede, U. K. and Fedorov, A. V.: Eastern equatorial Pacific warming delayed by aerosols and thermostat response to CO2 increase, Nature Climate Change, 11, 696–703, https://doi.org/10.1038/s41558-021-01101-x, number: 8 Publisher: Nature Publishing Group, 2021.

Heikenfeld, M., White, B., Labbouz, L., and Stier, P.: Aerosol effects on deep convection: the propagation of aerosol perturbations through convective cloud microphysics, Atmospheric Chemistry and Physics, 19, 2601–2627, https://doi.org/10.5194/acp-19-2601-2019, publisher: Copernicus GmbH, 2019.

https://doi.org/10.5194/egusphere-2024-1689
Preprint. Discussion started: 10 June 2024
© Author(s) 2024. CC BY 4.0 License.

Herbert, R. and Stier, P.: Satellite observations of smoke–cloud–radiation interactions over the Amazon rainforest, Atmospheric Chemistry and Physics, 23, 4595–4616, https://doi.org/10.5194/acp-23-4595-2023, publisher: Copernicus GmbH, 2023.

Herbert, R., Stier, P., and Dagan, G.: Isolating Large-Scale Smoke Impacts on Cloud and Precipitation Processes Over the Amazon With Convection Permitting Resolution, Journal of Geophysical Research: Atmospheres, 126, e2021JD034615, https://doi.org/10.1029/2021JD034615, _eprint: https://agupubs.onlinelibrary.wiley.com/doi/pdf/10.1029/2021JD034615, 2021.

Herbert, R. J.: Dataset for manuscript "Isolating aerosol-climate interactions in global kilometre-scale simulations", Zenodo [data set], https://doi.org/10.5281/zenodo.11470778, 2024.

Herbert, R. J., Bellouin, N., Highwood, E. J., and Hill, A. A.: Diurnal cycle of the semi-direct effect from a persistent absorbing aerosol layer over marine stratocumulus in large-eddy simulations, Atmospheric Chemistry and Physics, 20, 1317–1340, https://doi.org/10.5194/acp-20-1317-2020, publisher: Copernicus GmbH, 2020.

Hodzic, A. and Duvel, J. P.: Impact of Biomass Burning Aerosols on the Diurnal Cycle of Convective Clouds and Precipitation Over a Tropical Island, Journal of Geophysical Research: Atmospheres, 123, 1017–1036, https://doi.org/10.1002/2017JD027521, publisher: Blackwell Publishing Ltd, 2018.

Hohenegger, C., Kornblueh, L., Klocke, D., Becker, T., Cioni, G., Engels, J. F., Schulzweida, U., and Stevens, B.: Climate Statistics in Global Simulations of the Atmosphere, from 80 to 2.5 km Grid Spacing, Journal of the Meteorological Society of Japan. Ser. II, 98, 73–91, https://doi.org/10.2151/jmsj.2020-005, 2020.

Hohenegger, C., Korn, P., Linardakis, L., Redler, R., Schnur, R., Adamidis, P., Bao, J., Bastin, S., Behravesh, M., Bergemann, M., Biercamp, J., Bockelmann, H., Brokopf, R., Brüggemann, N., Casaroli, L., Chegini, F., Datseris, G., Esch, M., George, G., Giorgetta, M., Gutjahr, O., Haak, H., Hanke, M., Ilyina, T., Jahns, T., Jungclaus, J., Kern, M., Klocke, D., Kluft, L., Kölling, T., Kornblueh, L., Kosukhin, S., Kroll, C., Lee, J., Mauritsen, T., Mehlmann, C., Mieslinger, T., Naumann, A. K., Paccini, L., Peinado, A., Praturi, D. S., Putrasahan, D., Rast, S., Riddick, T., Roeber, N., Schmidt, H., Schulzweida, U., Schütte, F., Segura, H., Shevchenko, R., Singh, V., Specht, M., Stephan, C. C., von Storch, J.-S., Vogel, R., Wengel, C., Winkler, M., Ziemen, F., Marotzke, J., and Stevens, B.: ICON-Sapphire: simulating the components of the Earth system and their interactions at kilometer and subkilometer scales, Geoscientific Model Development, 16, 779–811, https://doi.org/10.5194/gmd-16-779-2023, publisher: Copernicus GmbH, 2023.

Hudson, J. G. and Yum, S. S.: Maritime–Continental Drizzle Contrasts in Small Cumuli, Journal of the Atmospheric Sciences, 58, 915–926, https://doi.org/10.1175/1520-0469(2001)058<0915:MCDCIS>2.0.CO;2, publisher: American Meteorological Society Section: Journal of the Atmospheric Sciences, 2001.

Illingworth, A. J., Barker, H. W., Beljaars, A., Ceccaldi, M., Chepfer, H., Clerbaux, N., Cole, J., Delanoë, J., Domenech, C., Donovan, D. P., Fukuda, S., Hirakata, M., Hogan, R. J., Huenerbein, A., Kollias, P., Kubota, T., Nakajima, T., Nakajima, T. Y., Nishizawa, T., Ohno, Y., Okamoto, H., Oki, R., Sato, K., Satoh, M., Shephard, M. W., Velázquez-Blázquez, A., Wandinger, U., Wehr, T., and van Zadelhoff, G.-J.: The EarthCARE Satellite: The Next Step Forward in Global Measurements of Clouds, Aerosols, Precipitation, and Radiation, Bulletin of the American Meteorological Society, 96, 1311 – 1332, https://doi.org/10.1175/BAMS-D-12-00227.1, 2015.

Jiang, J. H., Su, H., Huang, L., Wang, Y., Massie, S., Zhao, B., Omar, A., and Wang, Z.: Contrasting effects on deep convective clouds by different types of aerosols, Nature Communications, 9, 3874, https://doi.org/10.1038/s41467-018-06280-4, number: 1 Publisher: Nature Publishing Group, 2018.

Johnson, J. S., Cui, Z., Lee, L. A., Gosling, J. P., Blyth, A. M., and Carslaw, K. S.: Evaluating uncertainty in convective cloud microphysics using statistical emulation, Journal of Advances in Modeling Earth Systems, 7, 162–187, https://doi.org/10.1002/2014MS000383, _eprint: https://onlinelibrary.wiley.com/doi/pdf/10.1002/2014MS000383, 2015.

https://doi.org/10.5194/egusphere-2024-1689
Preprint. Discussion started: 10 June 2024
© Author(s) 2024. CC BY 4.0 License.

Kendon, E. J., Stratton, R. A., Tucker, S., Marsham, J. H., Berthou, S., Rowell, D. P., and Senior, C. A.: Enhanced future changes in wet and dry extremes over Africa at convection-permitting scale, Nature Communications, 10, 1794, https://doi.org/10.1038/s41467-019-09776-9, number: 1 Publisher: Nature Publishing Group, 2019.

Keshtgar, B., Voigt, A., Hoose, C., Riemer, M., and Mayer, B.: Cloud-radiative impact on the dynamics and predictability of an idealized extratropical cyclone, Weather and Climate Dynamics, 4, 115–132, https://doi.org/10.5194/wcd-4-115-2023, publisher: Copernicus GmbH, 2023.

Kinne, S.: Aerosol radiative effects with MACv2, Atmospheric Chemistry and Physics, 19, 10 919–10 959, https://doi.org/10.5194/acp-19-10919-2019, publisher: Copernicus GmbH, 2019.

Kinne, S., O'Donnel, D., Stier, P., Kloster, S., Zhang, K., Schmidt, H., Rast, S., Giorgetta, M., Eck, T. F., and Stevens, B.: MAC-v1: A new global aerosol climatology for climate studies, Journal of Advances in Modeling Earth Systems, 5, 704–740, https://doi.org/10.1002/jame.20035, _eprint: https://onlinelibrary.wiley.com/doi/pdf/10.1002/jame.20035, 2013.

Koch, D. and Del Genio, A. D.: Black carbon semi-direct effects on cloud cover: review and synthesis, Atmospheric Chemistry and Physics, 10, 7685–7696, https://doi.org/10.5194/acp-10-7685-2010, 2010.

Koren, I., Kaufman, Y. J., Remer, L. A., and Martins, J. V.: Measurement of the Effect of Amazon Smoke on Inhibition of Cloud Formation, Science, 303, 1342–1345, https://doi.org/10.1126/science.1089424, publisher: American Association for the Advancement of Science, 2004.

Koren, I., Vanderlei Martins, J., Remer, L. A., and Afargan, H.: Smoke invigoration versus inhibition of clouds over the amazon, Science, 321, 946–949, https://doi.org/10.1126/science.1159185, publisher: American Association for the Advancement of Science, 2008.

Langton, T., Stier, P., Watson-Parris, D., and Mulcahy, J. P.: Decomposing Effective Radiative Forcing Due to Aerosol Cloud Interactions by Global Cloud Regimes, Geophysical Research Letters, 48, e2021GL093 833, https://doi.org/10.1029/2021GL093833, _eprint: https://onlinelibrary.wiley.com/doi/pdf/10.1029/2021GL093833, 2021.

Lappin, F., de Boer, G., Klein, P., Hamilton, J., Spencer, M., Calmer, R., Segales, A. R., Rhodes, M., Bell, T. M., Buchli, J., Britt, K., Asher, E., Medina, I., Butterworth, B., Otterstatter, L., Ritsch, M., Puxley, B., Miller, A., Jordan, A., Gomez-Faulk, C., Smith, E., Borenstein, S., Thornberry, T., Argrow, B., and Pillar-Little, E.: Data collected using small uncrewed aircraft system during the TRacking Aerosol Convection Interactions ExpeRiment (TRACER), Earth System Science Data Discussions, 2023, 1–23, https://doi.org/10.5194/essd-2023-371, 2023.

Lauk, C. and Erb, K.-H.: Biomass consumed in anthropogenic vegetation fires: Global patterns and processes, Ecological Economics, 69, 301–309, https://doi.org/10.1016/j.ecolecon.2009.07.003, 2009.

Lebo, Z. J.: The Sensitivity of a Numerically Simulated Idealized Squall Line to the Vertical Distribution of Aerosols, Journal of the Atmospheric Sciences, 71, 4581–4596, https://doi.org/10.1175/JAS-D-14-0068.1, publisher: American Meteorological Society Section: Journal of the Atmospheric Sciences, 2014.

Leuenberger, D., Koller, M., Fuhrer, O., and Schär, C.: A generalization of the SLEVE vertical coordinate, Monthly Weather Review, 138, 3683–3689, https://doi.org/10.1175/2010MWR3307.1, publisher: American Meteorological Society, 2010.

Liu, L., Cheng, Y., Wang, S., Wei, C., Pöhlker, M., Pöhlker, C., Artaxo, P., Shrivastava, M., Andreae, M., Pöschl, U., and Su, H.: Impact of biomass burning aerosols on radiation, clouds, and precipitation over the Amazon during the dry season: dependence of aerosol-cloud and aerosol-radiation interactions on aerosol loading, Atmospheric Chemistry and Physics, pp. 1–50, https://doi.org/10.5194/acp-2020-191, 2020.

https://doi.org/10.5194/egusphere-2024-1689
Preprint. Discussion started: 10 June 2024
© Author(s) 2024. CC BY 4.0 License.

Lorenz, E. N.: Deterministic Nonperiodic Flow, Journal of the Atmospheric Sciences, 20, 130–141, https://doi.org/10.1175/1520-0469(1963)020<0130:DNF>2.0.CO;2, publisher: American Meteorological Society Section: Journal of the Atmospheric Sciences, 1963.

Ma, P.-L.: Enabling Aerosol-cloud interactions at GLobal convection-permitting scalES (EAGLES), EGU General Assembly, Vienna, Austria, https://doi.org/https://doi.org/10.5194/egusphere-egu24-12164, 2024.

Machado, L. A. T., Calheiros, A. J. P., Biscaro, T., Giangrande, S., Silva Dias, M. A. F., Cecchini, M. A., Albrecht, R., Andreae, M. O., Araujo, W. F., Artaxo, P., Borrmann, S., Braga, R., Burleyson, C., Eichholz, C. W., Fan, J., Feng, Z., Fisch, G. F., Jensen, M. P., Martin, S. T., Pöschl, U., Pöhlker, C., Pöhlker, M. L., Ribaud, J.-F., Rosenfeld, D., Saraiva, J. M. B., Schumacher, C., Thalman, R., Walter, D., and Wendisch, M.: Overview: Precipitation characteristics and sensitivities to environmental conditions during GoAmazon2014/5 and ACRIDICON-CHUVA, Atmospheric Chemistry and Physics, 18, 6461–6482, https://doi.org/10.5194/acp-18-6461-2018, 2018.

Mapes, B. and Neale, R.: Parameterizing Convective Organization to Escape the Entrainment Dilemma, Journal of Advances in Modeling Earth Systems, 3, https://doi.org/10.1029/2011MS000042, _eprint: https://onlinelibrary.wiley.com/doi/pdf/10.1029/2011MS000042, 2011.

Marinescu, P. J., Heever, S. C. v. d., Heikenfeld, M., Barrett, A. I., Barthlott, C., Hoose, C., Fan, J., Fridlind, A. M., Matsui, T., Miltenberger, A. K., Stier, P., Vie, B., White, B. A., and Zhang, Y.: Impacts of Varying Concentrations of Cloud Condensation Nuclei on Deep Convective Cloud Updrafts—A Multimodel Assessment, Journal of the Atmospheric Sciences, 78, 1147–1172, https://doi.org/10.1175/JAS-D-20-0200.1, publisher: American Meteorological Society Section: Journal of the Atmospheric Sciences, 2021.

Martin, S. T., Artaxo, P., Machado, L. A. T., Manzi, A. O., Souza, R. A. F., Schumacher, C., Wang, J., Andreae, M. O., Barbosa, H. M. J., Fan, J., Fisch, G., Goldstein, A. H., Guenther, A., Jimenez, J. L., Pöschl, U., Silva Dias, M. A., Smith, J. N., and Wendisch, M.: Introduction: Observations and Modeling of the Green Ocean Amazon (GoAmazon2014/5), Atmospheric Chemistry and Physics, 16, 4785–4797, https://doi.org/10.5194/acp-16-4785-2016, publisher: Copernicus GmbH, 2016.

Martins, J. A., Silva Dias, M. A. F., and Gonçalves, F. L. T.: Impact of biomass burning aerosols on precipitation in the Amazon: A modeling case study, Journal of Geophysical Research, 114, https://doi.org/10.1029/2007jd009587, publisher: American Geophysical Union (AGU), 2009.

McCoy, D. T., Bender, F. A.-M., Grosvenor, D. P., Mohrmann, J. K., Hartmann, D. L., Wood, R., and Field, P. R.: Predicting decadal trends in cloud droplet number concentration using reanalysis and satellite data, Atmospheric Chemistry and Physics, 18, 2035–2047, https://doi.org/10.5194/acp-18-2035-2018, publisher: Copernicus GmbH, 2018.

Miles, N. L., Verlinde, J., and Clothiaux, E. E.: Cloud Droplet Size Distributions in Low-Level Stratiform Clouds, Journal of the Atmospheric Sciences, 57, 295–311, https://doi.org/10.1175/1520-0469(2000)057<0295:CDSDIL>2.0.CO;2, publisher: American Meteorological Society Section: Journal of the Atmospheric Sciences, 2000.

Muller, C. J. and O'Gorman, P. A.: An energetic perspective on the regional response of precipitation to climate change, Nature Climate Change, 1, 266–271, https://doi.org/10.1038/nclimate1169, publisher: Nature Publishing Group, 2011.

Myhre, G., Kramer, R. J., Smith, C. J., Hodnebrog, Ø., Forster, P., Soden, B. J., Samset, B. H., Stjern, C. W., Andrews, T., Boucher, O., Faluvegi, G., Fläschner, D., Kasoar, M., Kirkevåg, A., Lamarque, J., Olivié, D., Richardson, T., Shindell, D., Stier, P., Takemura, T., Voulgarakis, A., and Watson-Parris, D.: Quantifying the Importance of Rapid Adjustments for Global Precipitation Changes, Geophysical Research Letters, 45, 11,399–11,405, https://doi.org/10.1029/2018GL079474, publisher: Blackwell Publishing Ltd, 2018.

NASA: Visible Earth, https://visibleearth.nasa.gov/collection/1484/blue-marble, 2024.

O'Gorman, P. A., Allan, R. P., Byrne, M. P., and Previdi, M.: Energetic Constraints on Precipitation Under Climate Change, Surveys in Geophysics, 33, 585–608, https://doi.org/10.1007/s10712-011-9159-6, publisher: Springer, 2012.

https://doi.org/10.5194/egusphere-2024-1689
Preprint. Discussion started: 10 June 2024
© Author(s) 2024. CC BY 4.0 License.

Palmer, T. and Stevens, B.: The scientific challenge of understanding and estimating climate change, Proceedings of the National Academy of Sciences, 116, 24 390–24 395, https://doi.org/10.1073/pnas.1906691116, publisher: Proceedings of the National Academy of Sciences, 2019.

Park, J. M. and van den Heever, S. C.: Weakening of tropical sea breeze convective systems through interactions of aerosol, radiation, and soil moisture, Atmospheric Chemistry and Physics, 22, 10 527–10 549, https://doi.org/10.5194/acp-22-10527-2022, publisher: Copernicus GmbH, 2022.

Pathak, R., Sahany, S., and Mishra, S. K.: Uncertainty quantification based cloud parameterization sensitivity analysis in the NCAR community atmosphere model, Scientific Reports, 10, 17 499, https://doi.org/10.1038/s41598-020-74441-x, number: 1 Publisher: Nature Publishing Group, 2020.

Pincus, R., Mlawer, E. J., and Delamere, J. S.: Balancing Accuracy, Efficiency, and Flexibility in Radiation Calculations for Dynamical Models, Journal of Advances in Modeling Earth Systems, 11, 3074–3089, https://doi.org/10.1029/2019MS001621, _eprint: https://onlinelibrary.wiley.com/doi/pdf/10.1029/2019MS001621, 2019.

Platnick, S., Hubanks, P., Meyer, K., and King, M. D.: MODIS Atmosphere L3 Monthly Product (08_L3), https://modis.gsfc.nasa.gov/data/dataprod/mod08.php, 2015.

Pringle, K. J., Carslaw, K. S., Spracklen, D. V., Mann, G. M., and Chipperfield, M. P.: The relationship between aerosol and cloud drop number concentrations in a global aerosol microphysics model, Atmospheric Chemistry and Physics, 9, 4131–4144, https://doi.org/10.5194/acp-9-4131-2009, publisher: Copernicus GmbH, 2009.

Proske, U., Ferrachat, S., Klampt, S., Abeling, M., and Lohmann, U.: Addressing Complexity in Global Aerosol Climate Model Cloud Microphysics, Journal of Advances in Modeling Earth Systems, 15, e2022MS003 571, https://doi.org/10.1029/2022MS003571, _eprint: https://onlinelibrary.wiley.com/doi/pdf/10.1029/2022MS003571, 2023.

Reick, C. H., Raddatz, T., Brovkin, V., and Gayler, V.: Representation of natural and anthropogenic land cover change in MPI-ESM, Journal of Advances in Modeling Earth Systems, 5, 459–482, https://doi.org/10.1002/jame.20022, _eprint: https://onlinelibrary.wiley.com/doi/pdf/10.1002/jame.20022, 2013.

Sand, M., Samset, B. H., Myhre, G., Gliß, J., Bauer, S. E., Bian, H., Chin, M., Checa-Garcia, R., Ginoux, P., Kipling, Z., Kirkevåg, A., Kokkola, H., Le Sager, P., Lund, M. T., Matsui, H., van Noije, T., Olivié, D. J. L., Remy, S., Schulz, M., Stier, P., Stjern, C. W., Takemura, T., Tsigaridis, K., Tsyro, S. G., and Watson-Parris, D.: Aerosol absorption in global models from AeroCom phase III, Atmospheric Chemistry and Physics, 21, 15 929–15 947, https://doi.org/10.5194/acp-21-15929-2021, publisher: Copernicus GmbH, 2021.

Sardeshmukh, P. D. and Hoskins, B. J.: The Generation of Global Rotational Flow by Steady Idealized Tropical Divergence, Journal of the Atmospheric Sciences, 45, 1228–1251, https://doi.org/10.1175/1520-0469(1988)045<1228:TGOGRF>2.0.CO;2, publisher: American Meteorological Society Section: Journal of the Atmospheric Sciences, 1988.

Sato, Y., Goto, D., Michibata, T., Suzuki, K., Takemura, T., Tomita, H., and Nakajima, T.: Aerosol effects on cloud water amounts were successfully simulated by a global cloud-system resolving model, Nature Communications, 9, 985, https://doi.org/10.1038/s41467-018-03379-6, number: 1 Publisher: Nature Publishing Group, 2018.

Savarin, A. and Chen, S. S.: Pathways to Better Prediction of the MJO: 1. Effects of Model Resolution and Moist Physics on Atmospheric Boundary Layer and Precipitation, Journal of Advances in Modeling Earth Systems, 14, e2021MS002 928, https://doi.org/10.1029/2021MS002928, _eprint: https://onlinelibrary.wiley.com/doi/pdf/10.1029/2021MS002928, 2022.

Seifert, A. and Beheng, K. D.: A two-moment cloud microphysics parameterization for mixed-phase clouds. Part 1: Model description, Meteorology and Atmospheric Physics, 92, 45–66, https://doi.org/10.1007/s00703-005-0112-4, publisher: Springer, 2006.

https://doi.org/10.5194/egusphere-2024-1689
Preprint. Discussion started: 10 June 2024
© Author(s) 2024. CC BY 4.0 License.

Shamekh, S., Lamb, K. D., Huang, Y., and Gentine, P.: Implicit learning of convective organization explains precipitation stochasticity, Proceedings of the National Academy of Sciences, 120, e2216158 120, https://doi.org/10.1073/pnas.2216158120, publisher: Proceedings of the National Academy of Sciences, 2023.

Sheffield, A. M., Saleeby, S. M., and van den Heever, S. C.: Aerosol-induced mechanisms for cumulus congestus growth, Journal of Geophysical Research: Atmospheres, 120, 8941–8952, https://doi.org/10.1002/2015JD023743, _eprint: https://onlinelibrary.wiley.com/doi/pdf/10.1002/2015JD023743, 2015.

Smagorinsky, J.: GENERAL CIRCULATION EXPERIMENTS WITH THE PRIMITIVE EQUATIONS: I. THE BASIC EXPERIMENT, Monthly Weather Review, 91, 99–164, https://doi.org/10.1175/1520-0493(1963)091<0099:GCEWTP>2.3.CO;2, publisher: American Meteorological Society Section: Monthly Weather Review, 1963.

Squires, P.: The Microstructure and Colloidal Stability of Warm Clouds, Tellus, 10, 256–261, https://doi.org/10.1111/j.2153-3490.1958.tb02011.x, _eprint: https://onlinelibrary.wiley.com/doi/pdf/10.1111/j.2153-3490.1958.tb02011.x, 1958.

Stevens, B., Giorgetta, M., Esch, M., Mauritsen, T., Crueger, T., Rast, S., Salzmann, M., Schmidt, H., Bader, J., Block, K., Brokopf, R., Fast, I., Kinne, S., Kornblueh, L., Lohmann, U., Pincus, R., Reichler, T., and Roeckner, E.: Atmospheric component of the MPI-M Earth System Model: ECHAM6, Journal of Advances in Modeling Earth Systems, 5, 146–172, https://doi.org/10.1002/jame.20015, _eprint: https://onlinelibrary.wiley.com/doi/pdf/10.1002/jame.20015, 2013.

Stevens, B., Fiedler, S., Kinne, S., Peters, K., Rast, S., Müsse, J., Smith, S. J., and Mauritsen, T.: MACv2-SP: a parameterization of anthropogenic aerosol optical properties and an associated Twomey effect for use in CMIP6, Geoscientific Model Development, 10, 433–452, https://doi.org/10.5194/gmd-10-433-2017, publisher: Copernicus GmbH, 2017.

Stevens, B., Satoh, M., Auger, L., Biercamp, J., Bretherton, C. S., Chen, X., Düben, P., Judt, F., Khairoutdinov, M., Klocke, D., Kodama, C., Kornblueh, L., Lin, S.-J., Neumann, P., Putman, W. M., Röber, N., Shibuya, R., Vanniere, B., Vidale, P. L., Wedi, N., and Zhou, L.: DYAMOND: the DYnamics of the Atmospheric general circulation Modeled On Non-hydrostatic Domains, Progress in Earth and Planetary Science, 6, 61, https://doi.org/10.1186/s40645-019-0304-z, 2019.

Stier, P., van den Heever, S. C., Christensen, M. W., Gryspeerdt, E., Dagan, G., Saleeby, S. M., Bollasina, M., Donner, L., Emanuel, K., Ekman, A. M. L., Feingold, G., Field, P., Forster, P., Haywood, J., and Kahn, R.: Multifaceted Aerosol Effects on Precipitation, Nature Geoscience, 2024.

Sullivan, S. C. and Voigt, A.: Ice microphysical processes exert a strong control on the simulated radiative energy budget in the tropics, Communications Earth & Environment, 2, 1–8, https://doi.org/10.1038/s43247-021-00206-7, number: 1 Publisher: Nature Publishing Group, 2021.

Tan, Z., Kaul, C. M., Pressel, K. G., Cohen, Y., Schneider, T., and Teixeira, J.: An Extended Eddy-Diffusivity Mass-Flux Scheme for Unified Representation of Subgrid-Scale Turbulence and Convection, Journal of Advances in Modeling Earth Systems, 10, 770–800, https://doi.org/10.1002/2017MS001162, _eprint: https://onlinelibrary.wiley.com/doi/pdf/10.1002/2017MS001162, 2018.

Taylor, K. E., Stouffer, R. J., and Meehl, G. A.: An Overview of CMIP5 and the Experiment Design, Bulletin of the American Meteorological Society, 93, 485 – 498, https://doi.org/10.1175/BAMS-D-11-00094.1, 2012.

Ten Hoeve, J. E., Remer, L. A., and Jacobson, M. Z.: Microphysical and radiative effects of aerosols on warm clouds during the Amazon biomass burning season as observed by MODIS: impacts of water vapor and land cover, Atmospheric Chemistry and Physics, 11, 3021–3036, https://doi.org/10.5194/acp-11-3021-2011, 2011.

https://doi.org/10.5194/egusphere-2024-1689
Preprint. Discussion started: 10 June 2024
© Author(s) 2024. CC BY 4.0 License.

Terai, C. R., Pritchard, M. S., Blossey, P., and Bretherton, C. S.: The Impact of Resolving Subkilometer Processes on Aerosol-Cloud Interactions of Low-Level Clouds in Global Model Simulations, Journal of Advances in Modeling Earth Systems, 12, e2020MS002 274, https://doi.org/10.1029/2020MS002274, _eprint: https://onlinelibrary.wiley.com/doi/pdf/10.1029/2020MS002274, 2020.

van der Werf, G. R., Randerson, J. T., Giglio, L., van Leeuwen, T. T., Chen, Y., Rogers, B. M., Mu, M., van Marle, M. J. E., Morton, D. C., Collatz, G. J., Yokelson, R. J., and Kasibhatla, P. S.: Global fire emissions estimates during 1997–2016, Earth System Science Data, 9, 697–720, https://doi.org/10.5194/essd-9-697-2017, publisher: Copernicus GmbH, 2017.

Varble, A. C., Nesbitt, S. W., Salio, P., Hardin, J. C., Bharadwaj, N., Borque, P., DeMott, P. J., Feng, Z., Hill, T. C. J., Marquis, J. N., Matthews, A., Mei, F., Öktem, R., Castro, V., Goldberger, L., Hunzinger, A., Barry, K. R., Kreidenweis, S. M., McFarquhar, G. M., McMurdie, L. A., Pekour, M., Powers, H., Romps, D. M., Saulo, C., Schmid, B., Tomlinson, J. M., van den Heever, S. C., Zelenyuk, A., Zhang, Z., and Zipser, E. J.: Utilizing a Storm-Generating Hotspot to Study Convective Cloud Transitions: The CACTI Experiment, Bulletin of the American Meteorological Society, 102, E1597 – E1620, https://doi.org/10.1175/BAMS-D-20-0030.1, 2021.

Wang, P., Yuval, J., and O'Gorman, P. A.: Non-Local Parameterization of Atmospheric Subgrid Processes With Neural Networks, Journal of Advances in Modeling Earth Systems, 14, e2022MS002 984, https://doi.org/10.1029/2022MS002984, _eprint: https://onlinelibrary.wiley.com/doi/pdf/10.1029/2022MS002984, 2022.

Watson-Parris, D. and Smith, C. J.: Large uncertainty in future warming due to aerosol forcing, Nature Climate Change, 12, 1111–1113, https://doi.org/10.1038/s41558-022-01516-0, number: 12 Publisher: Nature Publishing Group, 2022.

Weber, N. J. and Mass, C. F.: Subseasonal Weather Prediction in a Global Convection-Permitting Model, Bulletin of the American Meteorological Society, 100, 1079–1089, https://doi.org/10.1175/BAMS-D-18-0210.1, publisher: American Meteorological Society Section: Bulletin of the American Meteorological Society, 2019.

Weiss, P. and Stier, P.: Simulating the Earth system with interactive aerosols at the kilometer scale, EGU General Assembly, Vienna, Austria, https://doi.org/https://doi.org/10.5194/egusphere-egu24-2359, 2024.

Weiss, P., Herbert, R., and Stier, P.: A reduced complexity aerosol model for km-scale climate models, EGU General Assembly, Vienna, Austria, https://doi.org/https://doi.org/10.5194/egusphere-egu23-2082, 2023.

Wendisch, M., Poschl, U., Andreae, M. O., MacHado, L. A., Albrecht, R., Schlager, H., Rosenfeld, D., Martin, S. T., Abdelmonem, A., Afchine, A., Araujo, A. C., Artaxo, P., Aufmhoff, H., Barbosa, H. M., Borrmann, S., Braga, R., Buchholz, B., Cecchini, M. A., Costa, A., Curtius, J., Dollner, M., Dorf, M., Dreiling, V., Ebert, V., Ehrlich, A., Ewald, F., Fisch, G., Fix, A., Frank, F., Futterer, D., Heckl, C., Heidelberg, F., Huneke, T., Jakel, E., Jarvinen, E., Jurkat, T., Kanter, S., Kastner, U., Kenntner, M., Kesselmeier, J., Klimach, T., Knecht, M., Kohl, R., Kolling, T., Kramer, M., Kruger, M., Krisna, T. C., Lavric, J. V., Longo, K., Mahnke, C., Manzi, A. O., Mayer, B., Mertes, S., Minikin, A., Molleker, S., Munch, S., Nillius, B., Pfeilsticker, K., Pohlker, C., Roiger, A., Rose, D., Rosenow, D., Sauer, D., Schnaiter, M., Schneider, J., Schulz, C., De Souza, R. A., Spanu, A., Stock, P., Vila, D., Voigt, C., Walser, A., Walter, D., Weigel, R., Weinzierl, B., Werner, F., Yamasoe, M. A., Ziereis, H., Zinner, T., and Zoger, M.: Acridicon-chuva campaign: Studying tropical deep convective clouds and precipitation over amazonia using the New German research aircraft HALO, Bulletin of the American Meteorological Society, 97, 1885–1908, https://doi.org/10.1175/BAMS-D-14-00255.1, publisher: American Meteorological Society, 2016.

White, B., Gryspeerdt, E., Stier, P., Morrison, H., Thompson, G., and Kipling, Z.: Uncertainty from the choice of microphysics scheme in convection-permitting models significantly exceeds aerosol effects, Atmospheric Chemistry and Physics, 17, 12 145–12 175, https://doi.org/10.5194/acp-17-12145-2017, publisher: Copernicus GmbH, 2017.

https://doi.org/10.5194/egusphere-2024-1689
Preprint. Discussion started: 10 June 2024
© Author(s) 2024. CC BY 4.0 License.

Williams, A. I. L., Stier, P., Dagan, G., and Watson-Parris, D.: Strong control of effective radiative forcing by the spatial pattern of absorbing aerosol, Nature Climate Change, 12, 735–742, https://doi.org/10.1038/s41558-022-01415-4, number: 8 Publisher: Nature Publishing Group, 2022.

Williams, A. I. L., Watson-Parris, D., Dagan, G., and Stier, P.: Dependence of Fast Changes in Global and Local Precipitation on the Geographical Location of Absorbing Aerosol, Journal of Climate, 36, 6163–6176, https://doi.org/10.1175/JCLI-D-23-0022.1, publisher: American Meteorological Society Section: Journal of Climate, 2023.

Wood, R.: Stratocumulus Clouds, Monthly Weather Review, 140, 2373–2423, https://doi.org/10.1175/MWR-D-11-00121.1, 2012.

Wu, L., Su, H., and Jiang, J. H.: Regional simulations of deep convection and biomass burning over South America: 2. Biomass burning aerosol effects on clouds and precipitation, Journal of Geophysical Research Atmospheres, 116, https://doi.org/10.1029/2011JD016106, publisher: Blackwell Publishing Ltd, 2011.

Wu, M. and Lee, J.-E.: Thresholds for Atmospheric Convection in Amazonian Rainforests, Geophysical Research Letters, 46, 10 024–10 033, https://doi.org/10.1029/2019GL082909, _eprint: https://onlinelibrary.wiley.com/doi/pdf/10.1029/2019GL082909, 2019.

Yu, H., Fu, R., Dickinson, R. E., Zhang, Y., Chen, M., and Wang, H.: Interannual variability of smoke and warm cloud relationships in the Amazon as inferred from MODIS retrievals, Remote Sensing of Environment, 111, 435–449, https://doi.org/10.1016/j.rse.2007.04.003, publisher: Elsevier, 2007.

Zhang, S., Stier, P., and Watson-Parris, D.: On the contribution of fast and slow responses to precipitation changes caused by aerosol perturbations, Atmospheric Chemistry and Physics, 21, 10 179–10 197, https://doi.org/10.5194/acp-21-10179-2021, publisher: Copernicus GmbH, 2021.

Zängl, G., Reinert, D., Rípodas, P., and Baldauf, M.: The ICON (ICOsahedral Non-hydrostatic) modelling framework of DWD and MPI-M: Description of the non-hydrostatic dynamical core, Quarterly Journal of the Royal Meteorological Society, 141, 563–579, https://doi.org/10.1002/qj.2378, publisher: John Wiley and Sons Ltd, 2015.